Summer 2024

Effect of Ai–si Coating Weights on Corrosion and Weldability of Ultra-High-Strength Steel Usiborr 1500 Used in Automotive Structures

Hilary Anayochukwu Onyishi
Missouri University of Science and Technology

Department: Mechanical and Aerospace Engineering

EFFECT OF AI–SI COATING WEIGHTS ON CORROSION AND WELDABILITY OF ULTRA-HIGH-STRENGTH STEEL USIBOR^{R} 1500 USED IN AUTOMOTIVE STRUCTURES

by

HILARY ANAYOCHUKWU ONYISHI

A DISSERTATION

Presented to the Graduate Faculty of the

MISSOURI UNIVERSITY OF SCIENCE AND TECHNOLOGY

In Partial Fulfillment of the Requirements for the Degree

DOCTOR OF PHILOSOPHY

in

MECHANICAL ENGINEERING

2024

Approved by:

Dr. Anthony C. Okafor, Advisor
Dr. Lokeswarappa Dharani
Dr. K. Chandrashekhara
Dr. Jonghyun Park
Dr. V.A Samaranayake

PUBLICATION DISSERTATION OPTION

This dissertation consists of the following three articles, formatted in the style used by the Missouri University of Science and Technology:

Paper I, found on pages 11–30, has been published in *The International Journal of Corrosion Processes and Corrosion Control*, titled, "Effect of Ai-Si Coating Weights on Corrosion of Ultra-High-Strength Steel UsiborR 1500 Used in Automotive Structures". https://doi.org/10.1080/1478422X.2023.2245643.

Paper II, found on pages 31–57, has been published in *Advances in Materials and Processing Technologies*, titled, "Effect of Al-Si Coating Weights on Weldability of Hot-stamped Ultra-High-Strength Steel (UsiborR 1500) Used in Automotive Structures". https://doi.org/10.1080/2374068X.2023.2198833

Paper III, found on pages 58–89, has been published in *The International Journal of Advanced Manufacturing Technology*, titled, "Enhancement of viscosity and thermal conductivity of soybean vegetable oil using nanoparticles to form nanofluids for minimum quantity lubrication machining of difficult-to-cut metals".

ABSTRACT

There has been increased demand for hot-stamped pre-coated Usibor 1500R in automotive industries due to its excellent properties (ultra-high strength, weight reduction, low spring back and excellent corrosion protection). In this research work, investigation was conducted to better understand the effect of Ai-Si Coating Weights on weldability and corrosion of Ultra-High-Strength Steel Usibor 1500R used in Automotive Structures". The results show that weld nugget diameter increases with increasing weld current, better spot-weld nugget diameter is recorded at weld currents above 7.5 kA for both AS80 and AS150 and the weld current range decreases as the interdiffusion layer (IDL) thickness increases. With regards to the heat treatment, AS80 slightly shows a better weld range but heat treatment has no significant effect on welding of both AS80 and AS150, the weld diameter remained constant under the specified experimental conditions.

Both coating weights AS150 and AS80 exhibited similar excellent perforation corrosion resistance compared to 22MnB5 (Bare Usibor) due to highly protective corrosion products; AS80 and AS150 show maximum depth of corrosion attack less than 200 µm compared to 22MnB5 that has maximum depth of corrosion attack of 900 µm. AS150 displayed better resistance to cosmetic corrosion than AS80 due to thicker coating layer; AS80 coating shows higher resistance to red rust pitting corrosion than AS150 due to finer surface-morphology of AS80 as observed with SEM leading to a more homogeneous paint distribution, and E-coat thickness of 15 µm results in higher resistance to red-pitting corrosion than lower e-coat of 8 µm

ACKNOWLEDGMENTS

I would like to express my sincere gratitude and appreciation to my doctoral advisor, Dr. A. C. Okafor, for his continuous support, encouragement, and guidance through my doctoral process. My doctoral committee members, Dr. L. Dharani, Dr. K. Chandrashekhara, Dr. J. Park, and Dr. V. Sam, accepting to serve and take the time to review my work.

I would like to extend my sincere appreciation to my colleagues Raj Sohmshetty, and Igor Yakubtsov at Ford Motor Company for their collaborations, unwavering supports, and guidance throughout the research and experimental process at Ford Motor Company in Dearborn Michigan.

Finally, my sincere thanks to my entire family for their support. My beloved wife “Chidiebere”, and my beautiful and amazing kids “Somtochi, Kosiso, Ugonna and Chidubem” for their understanding of my absence. Their love, strength, and unwavering support carried me through. I appreciate and love you all.

TABLE OF CONTENTS

Page

LIST OF ILLUSTRATIONS

LIST OF TABLES

PAPER I Page

PAPER II

1. INTRODUCTION

Hot Stamping is the most viable and the most capable process for making B-pillars, impact beam, roof rails, and bumpers of automobile components from ultra-high-strength steels (UHSS). During the hot stamping process, coatings such as Al-Si and Zn, are usually applied to the surface of the UHSS sheets with the objectives of hindering decarbonization and surface oxidation to make the produced components more corrosion-resistant [1–3]. Presently in automotive industries, Aluminum and zinc-based coatings dominate hot stamping process. Wint et al [4] investigated galvanic corrosion of high strength low alloy (HSLA) steel laser welded to hot stamped UHSS used in automotive application in 0.017 M NaCl. They concluded that when HSLA steel was welded to heat treated (HT) UHSS (which is in martensitic state), anodic attack was only observed mainly on the UHSS grade and displayed a localized corrosion morphology. The pre-heat treated UHSS grade consisted of ferrite-pearlite microstructure. There are problems of liquid metal assisted cracking (LMAC) associated with Zinc coating that takes place during the coating process at the liquid phase. Zinc is brittle at ordinary temperatures; it has a low melting point of 420 °C which is very much lower than the hot stamping temperatures which is around 920 °C [5].

Once the liquid coating enters the base metal, it tends to crack the surface therefore the initiation of (LMAC), so the best way to avoid liquid metal assisted cracking is to use the indirect hot stamping process because the process allows the use of Zinc in a solid phase. ZnNi was commercialized as Gamma Protection coating though it has been discontinued and replaced by Aluminum-Silicon coated blanks. Choi and De

Cooman [6] studied the effects of decarburization of uncoated 22MnB5 steel. They found that the depth of the decarburization layer increases with time until the oxide layer forms a barrier between the steel and atmosphere. As the carbon is depleted in near-surface regions, the hardness is lowered. Ikeuchi and Yanagimoto [7] evaluated the effects of hot stamping process parameters on product properties using hot forming simulators. Their method utilized three systems for controlling the temperature history of the sheet, punch motion, and heat dissipation to the die, and permits to reproduce the hot stamping process and to correlate the forming conditions and the properties of the formed product. A numerical and experimental investigation of hot stamping of boron alloy heated steel was conducted by Naderi et al. [8] The paper reported that the die cooling media, i. e, water, or nitrogen, have a significant effect on material properties after hot stamping. They went further to conclude that using nitrogen as a coolant instead of water in the punch increases the yield strength by 50 to 65 MPa. Merklein and Lechler [9,10] investigated the thermo-mechanical properties of hot stamping steels. They concluded that increasing the temperature leads to significant decrease of the flow stress values and the slope of the initial strain hardening, and for the sensitivity of the material's forming properties regarding the strain rate, an increase of the deformation velocity leads to a significant increase of the stress levels and the work hardening. Boron alloy steel 22MnB5 with an Aluminum-Silicon coating layer named UsiborR 1500 was developed by ArcelorMittal and commonly used by automobiles companies in hot stamping [11][12]. Usibor 1500 is a hardenable alloy of boron steel coated with Aluminum-Silicon coating used in automobile parts especially when high strength is desired [13]. The manufacturing process is done in a press hardening line at this stage,

the steel blank is heated to 900 °C, formed, and then quenched to room temperature [14]. The outcome will produce a hardened part with a yield strength of 1100 MPa, and ultimate strength of 1500 MPa. Aluminum-silicon coating hinders steel from oxidation during heating and provides good corrosion protection for the parts. Previous investigations have been conducted to understand the impact of coating thickness on automobile bodies to prevent cosmetic and perforation corrosion in automotive parts. Allely et al [15] reported that formation of some corrosion elements is perceived to be due to a specific pH evolution during corrosion testing. In an ideal environment, corrosion may take many years to grow on riveted joints however accelerated corrosion testing can be a mechanism to replicate corrosion effects on the selected specimen on automotive components in real-time [16]. Hot stamping of boron alloy is a new technology in the automotive industry and provides advanced opportunity to produce pre-coated ultra-high strength steels with lighter weights [17][18]. This has provided avenues for auto makers to start investing lots of resources towards research for the purpose of generating wider knowledge base on hot stamping of boron alloy (Usibor 1500) that will support internal hot stamping production in auto industries.

Even though hot stamping is relatively a recent technology, there have been numerous publications on hot stamping of boron alloys but limited publications on effects of corrosion on indirect hot stamped Usibor 1500. Usibor 1500 presents unique challenges to automotive industries due to its desirable qualities and no research has been conducted in the past to examine the corrosion behavior of this two vital coating weights AS150 (150g/m^2) and AS80 (80 g/m^2) of Usibor 1500 formed through interdiffusion layer process. This paper presents a novel experimental investigation into

the corrosion behavior of two coating weights AS80 and AS150 of indirect hot-stamped Usibor 1500 used in assembly of automotive bodies. The experimental findings will be used to validate the cosmetic, perforating, and red pitting corrosion resistance performance specifications for automotive applications of hot stamped UsiborR 1500 that is used in making A-pillar, B-pillar, and bumper beams of automotive bodies at Ford Motor Inc.

Materials researchers are always looking for means to provide tougher materials used in engineering applications. These advanced materials need to be machined to their desired shape for specific applications. Cutting tools used during machining experience increased heat due to high friction and cutting forces generated at the cutting zone causing thermal softening of the cutting tool material, rapid tool wear, and shorter tool life. These adverse effects on the cutting tools also lead to reduced performance of the machined part due to reduced surface integrity such as high residual stresses and poor surface finish. Cutting fluids are used to improve surface integrity. The cutting fluid acts as a lubricant to reduce friction and as a coolant to cool the temperature at the cutting zone. Environmentally unfriendly conventional emulsion coolant (CEC) is the most effective cutting fluid for machining advanced materials like Inconel-718, titanium alloy, and compacted iron graphite used in aerospace, nuclear, and automotive industries. The viscosity and thermal conductivity of fluids used in these applications are of utmost importance to researchers and manufacturers and determine the suitability of the cutting fluid. Theoretical models have been proposed for determining these intrinsic properties, but these properties are best obtained by experimental investigation [1–3] due to the limitation of available models.

Nanofluids have been proposed to be an effective medium for transferring heat in applications such as heat exchangers, solar energy, and geothermal energy. Nanofluid is the suspension of nanoparticles in a base fluid to improve the thermal conductivity of the base fluid. The base fluid predominantly reported in the literature is water, but vegetable oil is attracting a lot of interest due to its advantages over water. The nanoparticles could be metallic or non-metallic, and the nanofluid so formed could be conventional nanofluid (single type of nanoparticle of the same average size) or hybrid nanofluid (multi-type of nanoparticles of same or different average sizes). Pryazhnikov et al. [4] studied thermal conductivity of nanofluids using different volumes up to 8%concentrations of SiO2, Al2O3, TiO2, ZrO2, and CuO and diamond nanoparticles of varying sizes up to 150 nm at room temperature and using water, ethylene glycol, and engine oil as base fluids. After comparing their results with existing models, they concluded that the thermal conductivity coefficient at room temperature is dependent on nanoparticle volume percentage, size, and property of the base fluid. Asadi et al. [5] studied the effect of adding hybrid nanoparticles (MgO-MWCNT) to engine oil to form nanofluid. They showed that by increasing hybrid nanoparticle mass concentration to 2% and increasing temperature to 50 °C, thermal conductivity can be enhanced by 65%. Omrani et al. [6] studied thermal conductivity and viscosity of multi-walled carbon nanotubes with different length and outer diameter sizes using a volume fraction of 0.05% and deionized water as base fluid. The result showed an enhancement of 36% and 5.5% in the thermal conductivity and viscosity, respectively. Chandrasekar et al. [7] investigated the thermal conductivity and viscosity of aluminum oxide/water nanofluid using 43 nm nanoparticle size at room temperature experimentally and theoretically.

Nanofluid at different volume percentages was prepared using a microwave-assisted chemical precipitation method and dispersion using a sonicator. It was observed that thermal conductivity and viscosity increased with volume concentration. Turgut et al. [8] investigated the effect of TiO2 nanoparticles with deionized water as base fluid on thermal conductivity and viscosity measurement of the formed nanofluid. The result showed an increase in thermal conductivity of 7.4% at a volume concentration of 3% at a temperature of 13 °C. They also observed that the increase in viscosity was higher than that predicted using the Einstein model. Vajjha and Das [9] experimentally investigated the thermal conductivity of aluminum oxide, copper oxide, and zinc oxide nanofluids using ethylene glycol and water mixture ratio 60:40 as base fluid. They also compared their results with those obtained using various existing models and observed that the results do not exhibit good agreement. Corcione [10] showed that effective thermal conductivity and dynamic viscosity of nanofluids are dependent on the size of the nanoparticle, base fluid, volume fraction of the nanoparticle, and application temperature. These factors make it very difficult to use existing viscosity and thermal conductivity models to theoretically determine the effective thermal conductivity and viscosity of different nanofluids.

Usually from 300 to 3000 l/h to the cutting zone, which provides the necessary lubrication and transfer of heat away from the cutting zone when machining, especially difficult-to-cut materials [11]. The frequent use of emulsion coolant has an adverse effect on the environment, machine operators, and the economy. Mineral resources are non-renewable, proper disposal of used emulsion coolant is difficult and very expensive, and machining operators with respiratory and skin diseases have been known to be

associated with constant exposure to mineral oil-based emulsion cutting fluids. The application of nanofluid in machining using emulsion coolant as base fluid is not feasible due to the large amount of fluid that is needed, the filtration system used during emulsion coolant application, and suppling the nanoparticle to the cutting zone will not be sustainable. Chetan et al. [12] investigated the application of alumina powder, colloidal solution of silver, and sunflower oil in water for use as nanofluid in the turning process. They observed that nanoparticles affect the contact angle, surface tension, droplet size, and spreadability of the fluid which also reduce tool wear and cutting forces. The present need for sustainable, renewable, biodegradable, and environmentally friendly cutting fluids has been at the forefront of research in machining for decades. The use of vegetable oil has found its niche in machining materials such as mild steel and aluminum alloys in the form of minimum quantity lubrication (MQL).

MQL is the application of a small amount of oil supplied to the cutting zone with the aid of pressurized air to form atomized molecules of oil in the air. In MQL machining, the air pressure breaks a precise amount of oil into droplets. The aerosol applied to the cutting zone via a nozzle forms a lubricating film, inhibits friction and heat growth, and flushes the chips away from the cutting zone. These methods have been very effective in machining soft materials like mild steel and aluminum alloys. In cutting difficult-to-cut metals, problems are still experienced due to a large amount of heat generated when machining materials like Inconel 718, compacted graphite iron, and titanium alloy. Recent studies have tried to solve such problems using cryogenic MQL [13–15], the application of cryogenic fluid in combination with MQL, or replacing pressurized shop air with chilled air. These procedures are associated with the hardening

of the materials and further increase cutting forces and tool breakage due to sudden cooling. Sidik et al. [16] conducted a review of the nanofluid application in MQL, and it was observed that most application has been on soft materials like steel, aluminum, and pure titanium; the base fluid has been deionized water, ethyl-glycol, and ester oil. Behera et al. [17] investigated the spreadability of metalworking fluid using aluminum oxide and different surfactants in deionized water during turning. The improvement in machinability was observed to be due to the spreadability of the nanofluid. Yuan et al. [18] investigated the influence of copper, silicon carbide, and diamond nanoparticles in different vegetable oil for use as nanofluid in end-milling of aluminum alloy using MQL application. It was observed that the nanofluid shows an improvement compared to dry machining by lowering cutting force and surface roughness. Li et al. [19] investigated the influence of graphene oxide nanofluid (graphene oxide suspended in commercially available synthetic ROCOL oil) on cutting temperature in machining Ti6Al4V. The result showed that the addition of nanoparticles reduced the cutting temperature and friction force.

Vegetable oils comprise mainly fatty acids that are either saturated or unsaturated. Saturated fatty acids have higher melting temperatures and most times solid at room temperature, while unsaturated fatty acids have low melting temperatures and tend to be liquid at room temperature. The viscosity and thermal conductivity of fluids used as the load-carrying fluid in moving parts and cooling medium in thermal applications are very important properties of the fluid. During machining of difficult-to-cut materials, the fluid in the cutting zone is subjected to shear stress and heat deformation due to shearing during chip formation. Viscosity and thermal conductivity

of fluids are dependent on the shear rate and temperature. When machine difficult-to-cut metals such as Inconel-718, lower cutting speeds are used, and high cutting temperatures are generated compared to the not difficult-to-cut metals such as aluminum and steel. In MQL machining, the pressure and flow rate are very low compared to conventional emulsion flood cooling, therefore, the need to supply fluids with enhanced viscosity without inhibiting the fluidity of the fluid. A recent study shows that increasing oleic (unsaturated) fatty acids composition in soybean, vegetable oil can enhance the viscosity of soybean oil but not the thermal conductivity [20]. From the above literature reviewed, knowledge of the effect of nanoparticles on intrinsic properties of vegetable oil for use in machining difficult-to-cut metal is lacking and needs to be investigated. To enhance the thermal conductivity of base vegetable oil for use in machining and understand its properties, AlO3, TiO2, and MoS2 nanoparticles of 30 nm nanoparticle size were added and uniformly suspended in high oleic soybean oil (HOSO) to form AlO3/HOSO-, TiO2/HOSO-, and MoS2/HOSO nanofluids to investigate the effect of type of nanoparticle of the same nanoparticle size, weight concentration, temperature on shear stability, suspension stability, viscosity, and thermal conductivity before their application in MQL machining of difficult-to-cut metals. Nanofluid-MQL or minimum quantity nano-lubrication is the application of MQL with nanoparticles in the base fluid. High oleic soybean oil has been shown to have the potential to replace mineral oil-based conventional emulsion flood coolant as a cutting fluid in the form of MQL application [21]. Modifying the fatty acid content of soybean oil is one method of increasing the viscosity of soybean oil. The method involves reducing the saturated fatty acid and polyunsaturated fatty acid contents which are solid at room temperature and have a high

oxidation rate, respectively. The method increases viscosity, oxidation stability, and shear stability without inhibiting the fluidity of the fluid. The influence of nanoparticles on rheological properties of nanofluid (viscosity and thermal conductivity) using high oleic soybean oil (HOSO) as the base fluid has never been investigated, and most of the nanofluid studies reported in the literature used water, engine oil, or ethyl glycol as base fluids in other applications such as heat transfer fluids, most of which are limited to room temperature.

This study investigated the influence of three types of nanoparticles (titanium oxide (TiO2), molybdenum disulfide (MoS2), and aluminum oxide (Al2O3)), varying nanoparticle weight concentration from 0.5 to 4%wt., and temperature range (25 to 70 °C) on shear stress, viscosity, thermal conductivity, and suspension stability of HOSO using the same 30 nm nanoparticle size in high oleic soybean vegetable oil as the base fluid for potential use in nanofluids minimum quantity lubrication (nMQL) machining of difficult-to-cut materials.

PAPER

I. EFFECT OF AI-SI COATING WEIGHTS ON CORROSION OF ULTRA-HIGH-STRENGTH STEEL USIBORR 1500 USED IN AUTOMOTIVE STRUCTURES

Hilary A. Onyishi[1,2,3], Anthony C. Okafor[1]*, Raj Sohmshetty[3]

Department of Mechanical and Aerospace Engineering, Missouri University of Science and Technology, 327 Toomey Hall, Rolla, MO-65409-005, USA

Collins Aerospace, 1 Hamilton Road Windsor Locks, CT 06096, USA

Ford Research and Innovation Center, 2101 Village Rd, Dearborn, MI 48124, USA

ABSTRACT

Corrosion has long been well known as one major factor that inhibits the longevity of automotive components especially in countries where a significant amount of salt is sprayed on highways during winter to improve driving conditions. In this paper, the effect of cosmetic, perforation and red pitting corrosion on indirect hot-stamped Ultra-High-Strength-Steel Usibor^{R} 1500 (22MnB5 with Al-Si coatings) were investigated using two different Al-Si coating weights AS80 (80g/m^2) and AS150 (150g/m^2). The experiments were conducted in a cyclic corrosion chamber over 12 weeks. The results show that both coating weights AS150 and AS80 exhibited similar excellent perforation corrosion resistance compared to 22MnB5 (Bare Usibor) due to highly protective corrosion products; Both AS80 and AS150 show maximum depth of corrosion attack less than 200 µm compared to 22MnB5 that has maximum depth of

corrosion attack of 900 µm. AS150 displayed better resistance to cosmetic corrosion than AS80 due to thicker coating layer; AS80 coating shows higher resistance to red rust pitting corrosion than AS150 due to finer surface-morphology of AS80 as observed with SEM leading to a more homogeneous paint distribution, and E-coat thickness of 15 µm results in higher resistance to red-pitting corrosion than lower e-coat of 8 µm.

1. INTRODUCTION

Hot Stamping is the most viable and the most capable process for making B-pillars, impact beam, roof rails, and bumpers of automobile components from ultra-high-strength steels (UHSS). During the hot stamping process, coatings such as Al-Si and Zn, are usually applied to the surface of the UHSS sheets with the objectives of hindering decarbonization and surface oxidation to make the produced components more corrosion-resistant [1–3]. Presently in automotive industries, Aluminum and zinc-based coatings dominate hot stamping process. Wint et al [4] investigated galvanic corrosion of high strength low alloy (HSLA) steel laser welded to hot stamped UHSS used in automotive application in 0.017 M NaCl. They concluded that when HSLA steel was welded to heat treated (HT) UHSS (which is in martensitic state), anodic attack was only observed mainly on the UHSS grade and displayed a localized corrosion morphology. The pre-heat treated UHSS grade consisted of ferrite-pearlite microstructure. There are problems of liquid metal assisted cracking (LMAC) associated with Zinc coating that takes place during the coating process at the liquid phase. Zinc is brittle at ordinary

temperatures; it has a low melting point of 420 °C which is very much lower than the hot stamping temperatures which is around 920 °C [5].

Once the liquid coating enters the base metal, it tends to crack the surface therefore the initiation of (LMAC), so the best way to avoid liquid metal assisted cracking is to use the indirect hot stamping process because the process allows the use of Zinc in a solid phase. ZnNi was commercialized as Gamma Protection coating though it has been discontinued and replaced by Aluminum-Silicon coated blanks. Choi and De Cooman [6] studied the effects of decarburization of uncoated 22MnB5 steel. They found that the depth of the decarburization layer increases with time until the oxide layer forms a barrier between the steel and atmosphere. As the carbon is depleted in near-surface regions, the hardness is lowered. Ikeuchi and Yanagimoto [7] evaluated the effects of hot stamping process parameters on product properties using hot forming simulators. Their method utilized three systems for controlling the temperature history of the sheet, punch motion, and heat dissipation to the die, and permits to reproduce the hot stamping process and to correlate the forming conditions and the properties of the formed product. A numerical and experimental investigation of hot stamping of boron alloy heated steel was conducted by Naderi et al. [8] The paper reported that the die cooling media, i. e, water, or nitrogen, have a significant effect on material properties after hot stamping. They went further to conclude that using nitrogen as a coolant instead of water in the punch increases the yield strength by 50 to 65 MPa. Merklein and Lechler [9,10] investigated the thermo-mechanical properties of hot stamping steels. They concluded that increasing the temperature leads to significant decrease of the flow stress values and the slope of the initial strain hardening, and for the sensitivity of the

material's forming properties regarding the strain rate, an increase of the deformation velocity leads to a significant increase of the stress levels and the work hardening. Boron alloy steel 22MnB5 with an Aluminum-Silicon coating layer named UsiborR 1500 was developed by ArcelorMittal and commonly used by automobiles companies in hot stamping [11][12]. Usibor 1500 is a hardenable alloy of boron steel coated with Aluminum-Silicon coating used in automobile parts especially when high strength is desired [13]. The manufacturing process is done in a press hardening line at this stage, the steel blank is heated to 900 °C, formed, and then quenched to room temperature [14]. The outcome will produce a hardened part with a yield strength of 1100 MPa, and ultimate strength of 1500 MPa. Aluminum-silicon coating hinders steel from oxidation during heating and provides good corrosion protection for the parts. Previous investigations have been conducted to understand the impact of coating thickness on automobile bodies to prevent cosmetic and perforation corrosion in automotive parts. Allely et al [15] reported that formation of some corrosion elements is perceived to be due to a specific pH evolution during corrosion testing. In an ideal environment, corrosion may take many years to grow on riveted joints however accelerated corrosion testing can be a mechanism to replicate corrosion effects on the selected specimen on automotive components in real-time [16]. Hot stamping of boron alloy is a new technology in the automotive industry and provides advanced opportunity to produce pre-coated ultra-high strength steels with lighter weights [17][18]. This has provided avenues for auto makers to start investing lots of resources towards research for the purpose of generating wider knowledge base on hot stamping of boron alloy (Usibor 1500) that will support internal hot stamping production in auto industries.

Even though hot stamping is relatively a recent technology, there have been numerous publications on hot stamping of boron alloys but limited publications on effects of corrosion on indirect hot stamped Usibor 1500. Usibor 1500 presents unique challenges to automotive industries due to its desirable qualities and no research has been conducted in the past to examine the corrosion behavior of this two vital coating weights AS150 (150g/m^2) and AS80 (80 g/m^2) of Usibor 1500 formed through interdiffusion layer process. This paper presents a novel experimental investigation into the corrosion behavior of two coating weights AS80 and AS150 of indirect hot-stamped Usibor 1500 used in assembly of automotive bodies. The experimental findings will be used to validate the cosmetic, perforating, and red pitting corrosion resistance performance specifications for automotive applications of hot stamped UsiborR 1500 that is used in making A-pillar, B-pillar, and bumper beams of automotive bodies at Ford Motor Inc.

1.1. EXPERIMENTAL SET-UP AND PROCEDURES

The experimental tests were carried out on indirect hot-stamped Usibor^R 1500 of 1.5 mm gage thickness with two different coating weights of AS150 (36µm Al-Si coating thickness) and AS80 (20µm Al-Si coating thickness) which are equivalent to AS150 (150g/m^2) and AS80 (80 g/m^2) respectively. These two most common coating weights used in automobile industries were developed by ArcelorMittal in 2013 with the rationale to (i) lower cost and be more competitive and (ii) introduce a coating weight that would minimize the heating/dwell time in the ovum [19]. Tables 1 and 2 show the chemical composition and mechanical properties respectively of Usibor 1500. A couple

of years ago, most automotive industries usually use salt spray tests (SST) to conduct quick corrosion evaluation methods, it was later discovered that the salt spray test has poor reliability and does not show a good correlation with actual environmental conditions. Automotive industries have widely adopted cyclic corrosion tests (CCT) which comprises both “wet” and “dry” conditions in addition to the salt spray test (SST) as the standard method that realistically produces the natural corrosion conditions. Despite the increasing research by automotive industries to understand and checkmate two major types of corrosion (cosmetic and perforation) that attack automobile bodies, corrosion is still a major challenge in automotive industries. **Cosmetic corrosion** can be defined as the type of corrosion that occurs mainly on the outer panels of automotive bodies whereas **perforation corrosion** is related to the type of corrosions that occurs at the joined regions or area not exposed in automotive bodies; the magnitude of the coating weights plays a vital role in the effectiveness of cosmetic corrosion resistance performance of automotive body panels. Table 3 shows the coating designations of AS80 and AS150 test coupons of Usibor 1500.

Table 1. Chemical Composition of Usibor 1500

Element	C	Si	Mn	P	S	Al	Cr	Ti	B	Ni	Mo	Cu
Wt.%	0.3	0.3	1.4	0.02	0.005	0.05	0.2	0.05	0.004	0.1	0.1	0.1

Table 2. Mechanical properties of Usibor 1500

Properties	Values
Elongation (%)	≤ 6
Tensile Strength (MPa)	1500
Yield Strength (MPa)	1000
Microstructure	Martensite

Table 3. AS150 and AS80 Coating Designation and Thickness Requirements

Coating Designations	Condition	Total Coating Thickness (g/m^2)	Inter-diffusion Layer (IDL) Thickness (μm)
AS150	Press-hardened	150	≤16
AS80	Press-hardened	80	≤12

1.2. MATERIALS PREPARATION

The Aluminum-Silicon coating on the as-received boron steel sheet was approximately 30 μm double-sided, the mechanism of aluminum-based coating of AS 150 and AS80 was achieved through an interlayer diffusion process which involved pre-coating the blank of Usibor^R 1500. The blank was heated at an elevated temperature of 920 °C which enabled the iron diffusion to take place within 4-6 minutes in the furnace, forming AlSiFe layers as shown in Figure 1. The iron diffusion was a short-monitored heating time process. Silicon composition was about 10% and 90% Aluminum. Fan and De Cooman [20] reported that the coating could crack easily but the cracks would not extend to the diffusion layer, therefore, the thickness of the diffusion layer is vital and must be managed effectively. This was achieved by controlling the furnace temperature

and dwell time. Five sub-layers in Figure 1. indicated the dominant phases of Layer 1 in the as-received steel sheet were (Al) matrix and Al-Si, while the dominant phase of Layer 2 was Fe2Al7Si ternary intermetallic compound. After the hot stamping process, three new phases are formed. The new phases are Fe (Al, Si), Fe (Al, Si)2, and Fe, they differ by the Aluminum, cracks are present in the Al-Si–Fe top coating after the forming process. The presence of microcracks could be emanating due to the presence of a η-Fe2Al5 compound in the highly aluminized layer which is susceptible to the thermal stress at the time of heating and cooling Suehiro et al [21]. The 10% silicon was added to the coating to create elastic layers in the coating, however, without the addition of silicon, the coating will be extremely hard and easy to break[22]

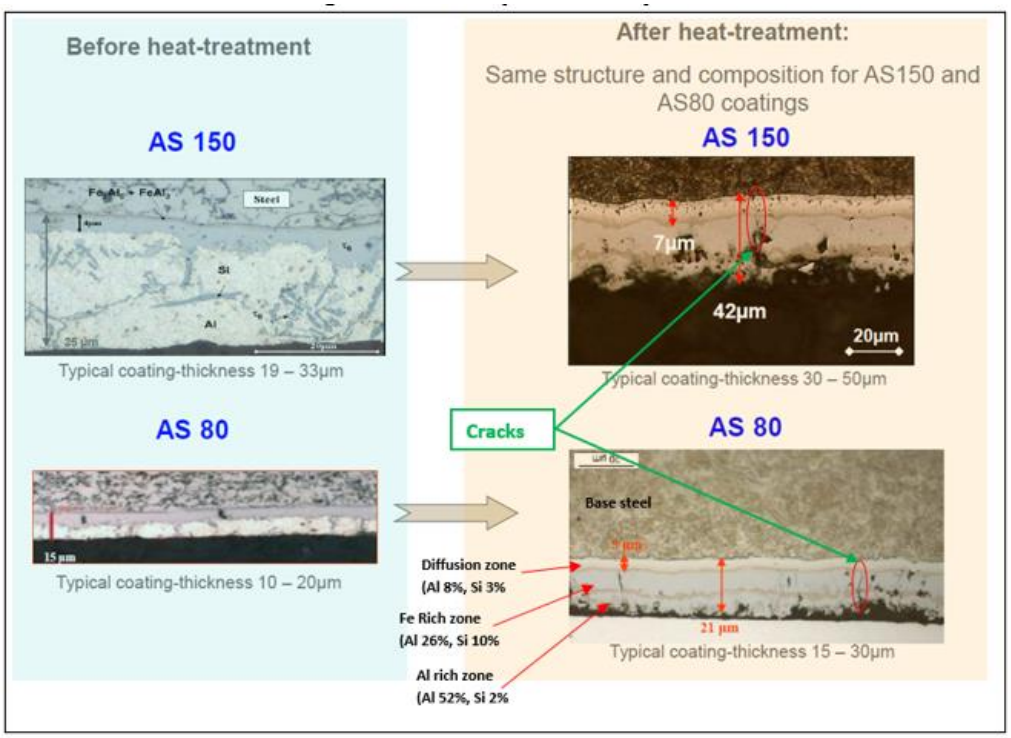

Figure 1. The coating weight characteristics of AS150 and AS80.

1.3. EXPERIMENTAL PROCEDURE

Test specimens used were Usibor^{R} 1500 with two different coating weights AS150 (150g/m^2) and AS80 (80g/m^2), as-received Boron alloy steel 22MnB5 (Bare Usibor), and galvanized High-Strength Low Alloy (HSLA). Also, additional specimen used during the experiment was a low electrocoated (e-coat) paint thickness (8µm and 15µm) of AS150 and AS80 for reference purposes only. Indirect hot-stamped Usibor^{R} 1500 coated with two different coating weights AS150 and AS80 that were developed by Interdiffusion layer mechanism processes were cut into smaller test coupons. All the specimens were cut into small test coupons, placed into the cyclic corrosion chamber, and orientated at a horizontal angle of 65° to 75° with the sides to be investigated facing upward direction. Cyclic corrosion test chamber shown in Figure 2, the chamber is effective in yielding results that resembles what happens in real life corrosion environment because it creates well-controlled conditions that are practical to exhibit salt spray tests over conventional exposures. Salt solution of 1 % sodium chloride (NaCl) was sprayed every hour. The volume of 3ml is considered low salt spray phase duration and was sprayed periodically for each 48 hours cycle time window. For every completed cycle, the specimens were removed and checked for corrosion resistance performance with the help of laser blue line triangulation scanner. The triangulation scanner is a high functioning 2D/3D profile sensor with integrated intelligence in the head region that facilitates varieties of measuring tasks at great precision and measuring rate. The laser blue line triangulation method helps to detect, measure, and evaluate profiles on different object surfaces without coming in close contact with the surface. This method was crucial in helping us evaluate the magnitude of corrosion attack in

depth, the mean scribe creep-back (mm), maximal scribe creep-back(mm) and maximal pitting in scribe lines(μm) after each cycle time of perforation, cosmetic and the red rust pitting VDA corrosion tests. The process was continued for all the specimens in an accelerated manner. Cyclic corrosion test as the name suggests involves different climate conditions which are cycled. The procedure is widely accepted in automotive industries because it represents the failure that might occur naturally in an accelerated manner [23].

Figure 2. Accelerated corrosion test chambers used for UsiborR AS150 and AS80 coupons.

There are distinct types of test standards to select from to be able to characterize the susceptibility of a material combination of the most important lightweight design structural materials like boron alloy and assess the protective effect of coatings [24]. An associated air temperature conditioning unit permits testing to be performed at -15 °C to

50 °C temperature range as displayed graphically as shown in Figure 3 This process expansion is fundamentally needed in investigations of corrosion effects according to German technical standard VDA 233-102 (version 02/2008) for substances in parts and materials for the automotive industry), more especially as -15 °C is classified as a cold phase. Additionally, infiltration impact on corrosion can also be distinguished through a condition that is reproducible by the means of expanded natural weathering range of temperature in fractions of the testing.

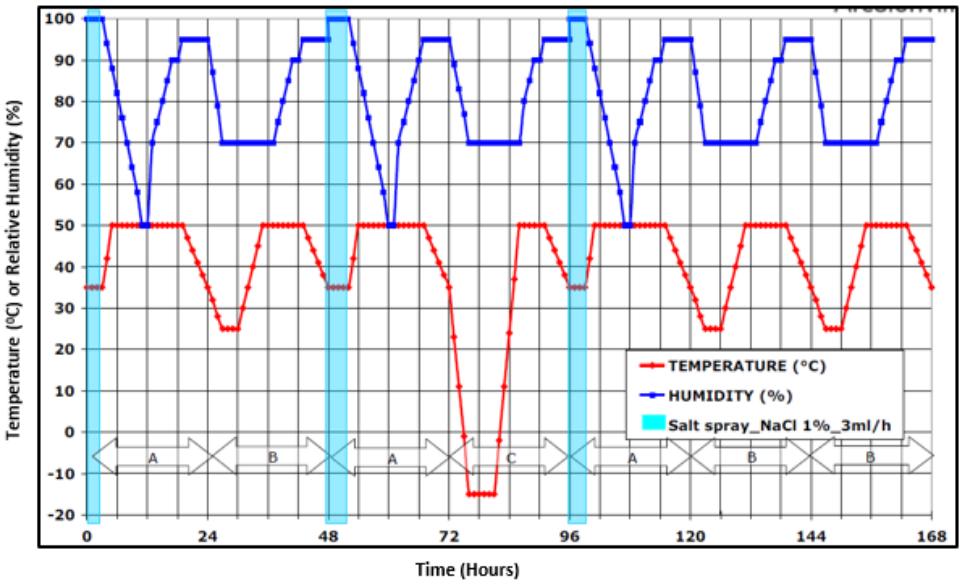

Figure 3. Temperature and humidity change during cycles of the VDA test.

However measurement of perforation in steel substrates by laser triangulation after twelve new VDA weeks indicates that during cyclic corrosion testing within 2 weeks of the testing process, AlSi and steel oxidized simultaneously in cracks after 6 weeks of the testing, SEM indicated that cracks were filled with high inhibiting corrosion products

(Al-Fe-Si hydroxides) precipitates as PH increases as a result of oxygen reduction, however, attacks in depth were very limited as shown in Figure 4. As the corrosion testing progressed to 12 weeks period, the maximum attack on depths was still less than 70(μm) due to the compactness of the corrosion product layers blocking the oxygen diffusion through the steel surface thereby slowing down the corrosion propagation in the steel cavity of Usibor^{R} AluSi. In addition, the presence of cracks in the coating down to the substrate means that not only the barrier effect of the coating is tested, but also the sacrificial protection and corrosion products inhibition. **Cosmetic corrosion** comprising blistering and scabbing took place on the exterior surfaces, where the paint film tends to be destroyed, the measurements of experimental results for all the samples were recorded and analyzed in each case of perforating, cosmetic and red rust spitting corrosion resistance.

2. RESULTS AND DISCUSSIONS

2.1. PERFORATING CORROSION RESISTANCE OF UHSS USIBOR, AS80, AS150 AND 22MNB5 (BARE USIBOR)

Figure 5. shows perforating corrosion testing on UHSS Usibor AS80, AS150 and 22MnB5 (Bare Usibor) non-painted specimens. The result shows that AS150 and AS80 with 80g/m^2 and 150g/m^2 double sided coating exhibited similar excellent perforation corrosion resistance due to highly protective corrosion products compared with 22MNB5 (Bare Usibor). The results of the perforation corrosion test in non-uniform assemblies when Al-Si coated Usibor AS150, AS80, or 22MnB5 with galvanized DP600 are displayed, the x-axis shows the material composition of the assembly, and the depth

attack (µm) was recorded on the vertical axis. The bare Usibor 1500 22MnB5 materials showing the highest corrosion depths of ~900 µm were noted. Comparing the first 2 histograms AS80 and AS150, even though AS150 has slightly higher depth of attack than AS80, the two materials display a high level of corrosion resistance when compared to the level for bare Usibor 22MnB. Both AS80 and AS150 show maximum depth of corrosion attack of less than 200 µm compared to 22MnB5 that has maximum depth of corrosion attack of approximately 900 µm.

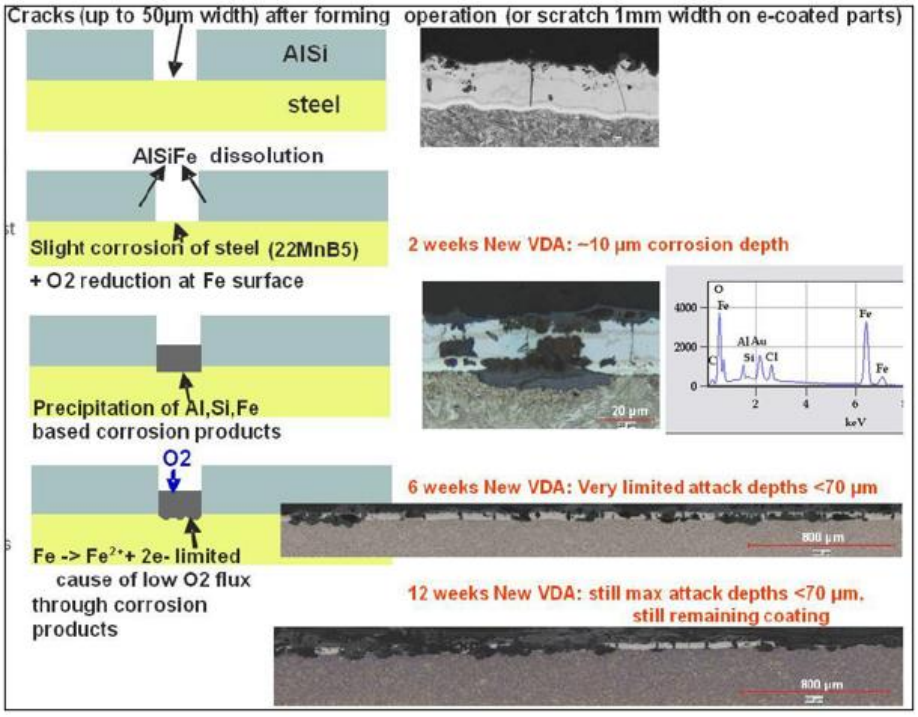

Figure 4. UsiborR 1500 corrosion and cracks formation vs VDA weeks corrosion exposure.

This good performance was due to barrier effects of corrosion products, AS80 is as good as AS150 for perforation corrosion resistance but slightly much better.

2.2. COSMETIC CORROSION RESISTANCE OF AS80 AND AS150

Cosmetic corrosion comprising blistering and scabbing takes place on the exterior surfaces, where the paint film tends to be destroyed. The effect of chemical conversion coating and electrode deposition (ED) coating on an automotive component of Usibor 1500 with two coating weights AS150 and AS80 was studied. In Figure 6, the new VDA cosmetic corrosion test measured by laser triangulation shows attack on the depth in the scribe lines, comparing the mean scribe creep back (mm) on the vertical axis for the first three materials, it could be observed that Usibor AS150 performed better than AS80 in terms of mean and maximum scribed creep back (mm) of scribed lines, but cosmetic corrosion attack was deeper on bare Usibor 22MnB5 however, the damage by the scribe line after corrosion exposure is more on AS80 compared to that of AS150

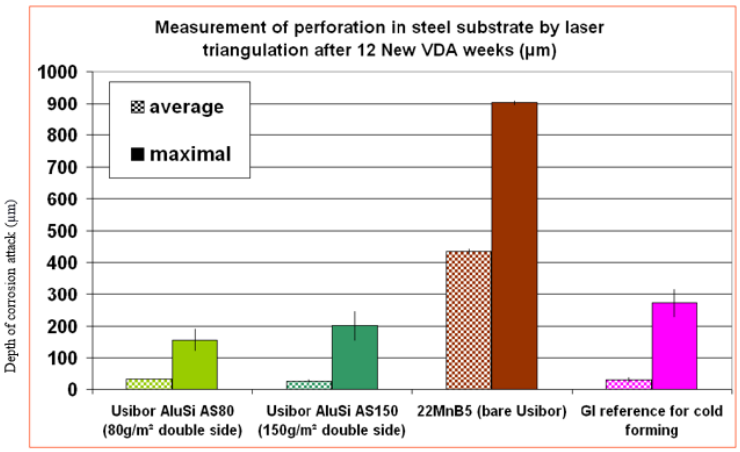

Figure 5. Corrosion attack depth measured by laser triangular.

The result shows Usibor AS150 displayed better resistance to cosmetic corrosion than Usibor AS80 due to the presence of an aluminum-rich protective corrosion product.

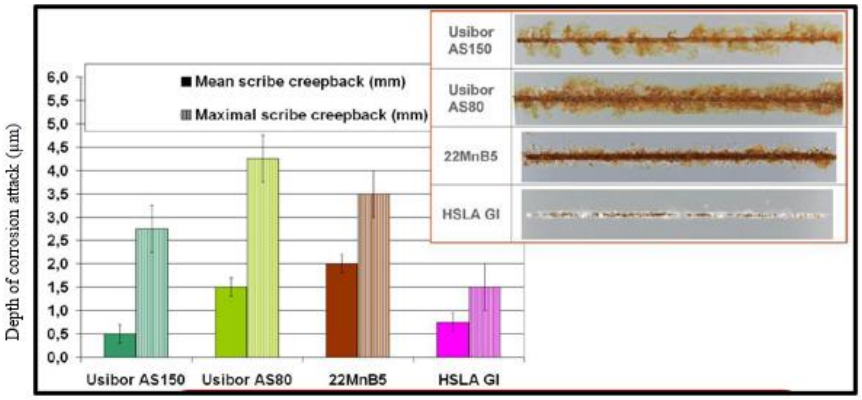

Figure 6. Cosmetic corrosion results of Usibor Al-Si AS80, Usibor Al-Si A150 and 22MnB5

2.3. CORROSION TESTS WITH LOW E-COAT THICKNESSES TO STUDY RED RUST PITTING OF AS80 AND AS150

Corrosion tests with low e-coat thicknesses of less than 20 µm were performed through electrode-deposit (ED) of 8(µm) and 15(µm) respectively on AS150 and AS80 to study red rust pitting as shown in Figure 7. The better behavior of AS80 by low e-coat thickness is explained by a finer surface-morphology of AS80 as observed with SEM, as shown in Figure 8, which leads to a more homogeneous paint distribution in areas with low paint thickness resulting in better corrosion resistance performance with red rust pitting.

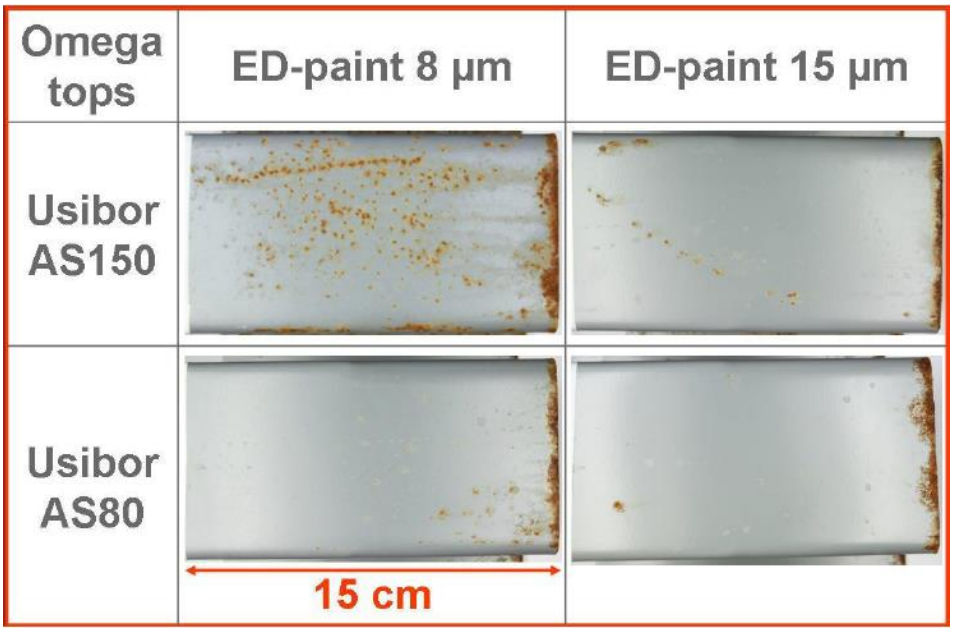

Figure 7. Corrosion tests with low E-coat thicknesses.

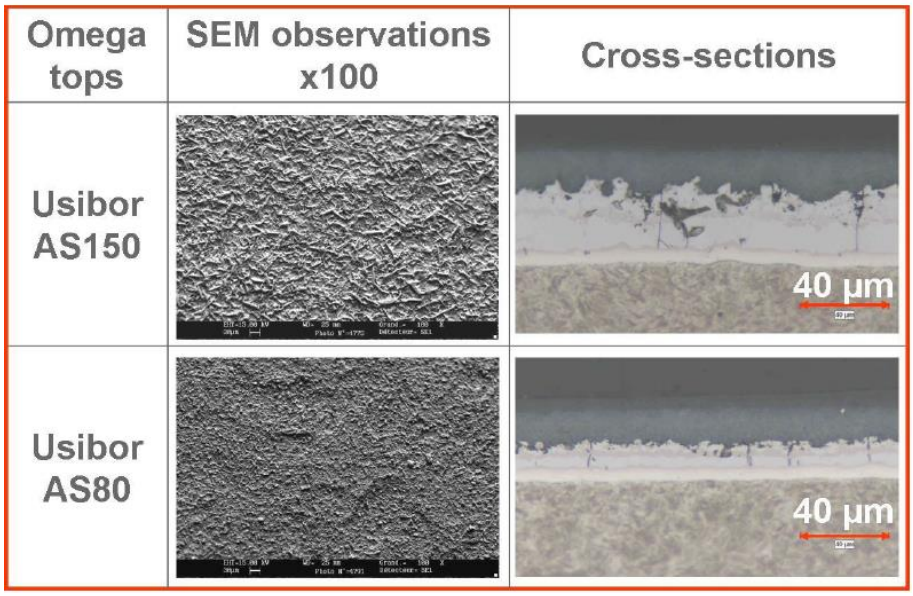

Figure 8. Corrosion-tests with low e-coat thickness <20µm) observed with SEM.

3. CONCLUSION

3.1. CONCLUSION AND FUTURE WORK

In this paper, corrosion analysis of hot stamped Usibor^{R} 1500 coated with two different coating weights AS150 (36µm) and AS80 (20µm) using the Interdiffusion Layer process is studied. The result shows: Both coating weights AS150 and AS80 exhibited similar excellent perforation corrosion resistance compared to 22MnB5 (Bare Usibor) due to highly protective corrosion products of Aluminum-Silicon (AlSi). Both AS80 and AS150 show maximum depth of corrosion attack of less than 200 µm compared to 22MnB5 that has maximum depth of corrosion attack of approximately 900 µm. The Aluminum-Silicon coating of Usibor^{R} 1500 serves as a barrier to oxygen reduction to a greater magnitude even when the corrosion element is perceived to be gradually initiating corrosion attack into steel cavities of the alloy.

The result of the cosmetic corrosion test shows Usibor AS150 displayed better resistance to cosmetic corrosion than Usibor AS80, in terms of mean and maximum scribed creep back (mm) of scribed lines, due to the presence of aluminum -rich protective corrosion product. Thicker coating layer thus implies the thicker the coating weight the better the corrosion resistance. The result agrees with Mizuno [25] finding that an increase in the coating thickness improves corrosion resistance.

The results of the red rust pitting corrosion test show that AS80 coating shows higher resistance to red-pitting corrosion than AS150 due to finer surface-morphology of AS80 as observed with SEM leading to a more homogeneous paint distribution.

Also, thicker ED paint of e-coat thickness of 15 µm results to higher resistance to red-pitting corrosion compared to lower e-coat thickness of 8 µm.

3.2. FUTURE WORK

Coupled with cost reduction opportunities, further research work should be conducted to study the feasibility of a stack up of AS80 and AS80 with 1.5mm and 1mm gage to avoid unexpected production or parts performance issues. Also, corrosion studies of resistance spot welded joints of USIBOR 150 with AS80 coatings to ascertain their corrosion resistance, types, and mechanism.

REFERENCES

[1] A. Turetta, S. Bruschi, A. Ghiotti, Investigation of 22MnB5 formability in hot-stamping operations, J Mater Process Technol. (2006). https://doi.org/10.1016/j.jmatprotec.2006.04.041.

[2] C. Kim, M.J. Kang, Y.D. Park, Laser welding of Al-Si coated hot stamping steel, in: Procedia Eng, Elsevier Ltd, 2011: pp. 2226–2231. https://doi.org/10.1016/j.proeng.2011.04.368.

[3] D.J. Penney, J.H. Sullivan, D.A. Worsley, Investigation into the effects of metallic coating thickness on the corrosion properties of Zn-Al alloy galvanising coatings, Corros Sci. 49 (2007) 1321–1339. https://doi.org/10.1016/j.corsci.2006.07.006.

[4] N. Wint, J. Leung, J.H. Sullivan, D.J. Penney, Y. Gao, The galvanic corrosion of welded ultra-high strength steels used for automotive applications, Corros Sci. 136 (2018) 366–373. https://doi.org/10.1016/j.corsci.2018.03.025.

[5] E. Billur, C. Wang, C. Bloor, M. Holecek, H. Porzner, T. Altan, Advancements in tailored hot stamping simulations: Cooling channel and distortion analyses, in: 2014. https://doi.org/10.1063/1.4850158.

[6] W.S. Choi, B.C. De Cooman, Characterization of the bendability of press-hardened 22MnB5 steel, Steel Res Int. (2014). https://doi.org/10.1002/srin.201300276.

[7] K. Ikeuchi, J. Yanagimoto, Valuation method for effects of hot stamping process parameters on product properties using hot forming simulator, J Mater Process Technol. (2011). https://doi.org/10.1016/j.jmatprotec.2011.03.017.

[8] M. Naderi, V. Uthaisangsuk, U. Prahl, W. Bleck, A Numerical and Experimental Investigation into Hot Stamping of Boron Alloyed Heat Treated Steels, Steel Res Int. (2008). https://doi.org/10.1002/srin.200806320.

[9] M. Merklein, J. Lechler, Investigation of the thermo-mechanical properties of hot stamping steels, J Mater Process Technol. (2006). https://doi.org/10.1016/j.jmatprotec.2006.03.233.

[10] M. Tisza, Korszerű, nagy szilárdságú autóipari acélok fejlesztése, Acta Materialia Transylvanica Magyar Kiadás. 4 (2021) 9–17. https://doi.org/10.33923/amt-2021-01-02.

[11] X. Bano, J.P. Laurent, Heat treated boron steels in the automotive industry, in: Mechanical Working and Steel Processing Conference Proceedings, 1997.

[12] L. Vaissiere, J.P. Laurent, A. Reinhardt, Development of pre-coated boron steel for applications on PSA peugeot citroën and RENAULT bodies in white, in: SAE Technical Papers, 2002. https://doi.org/10.4271/2002-01-2048.

[13] W. Lin, F. Li, X. Hua, D. Wu, Effect of filler wire on laser welded blanks of Al-Si-coated 22MnB5 steel, J Mater Process Technol. 259 (2018) 195–205. https://doi.org/10.1016/j.jmatprotec.2018.04.041.

[14] T. Kurz, G. Luckeneder, T. Manzenreiter, H. Schwinghammer, A. Sommer, Zinc Coated Press-Hardening Steel - Challenges and Solutions, in: SAE Technical Papers, 2015. https://doi.org/10.4271/2015-01-0565.

[15] C. Allély, L. Dosdat, O. Clauzeau, K. Ogle, P. Volovitch, Anticorrosion mechanisms of aluminized steel for hot stamping, Surf Coat Technol. (2014). https://doi.org/10.1016/j.surfcoat.2013.10.072.

[16] A.C. Okafor, C. Nnadili, Evaluation of the effects of corrosion on fatigue life of clad aluminum alloy 2024-T3-riveted lap joints with acoustic emission monitoring, Journal of Failure Analysis and Prevention. (2012). https://doi.org/10.1007/s11668-012-9606-9.

[17] H. Karbasian, A.E. Tekkaya, A review on hot stamping, J Mater Process Technol. (2010). https://doi.org/10.1016/j.jmatprotec.2010.07.019.

[18] R. Neugebauer, F. Schieck, S. Polster, A. Mosel, A. Rautenstrauch, J. Schönherr, N. Pierschel, Press hardening - An innovative and challenging technology, Archives of Civil and Mechanical Engineering. (2012). https://doi.org/10.1016/j.acme.2012.04.013.

[19] Hot Stamping of Ultra High-Strength Steels, 2019. https://doi.org/10.1007/978-3-319-98870-2.

[20] D.W. Fan, B.C. De Cooman, State-of-the-knowledge on coating systems for hot stamped parts, Steel Res Int. (2012). https://doi.org/10.1002/srin.201100292.

[21] M. Suehiro, J. Maki, K. Kusumi, M. Ohgami, T. Miyakoshi, Properties of aluminized steels for hot-forming, in: SAE Technical Papers, 2003. https://doi.org/10.4271/2003-01-2853.

[22] H. Onyishi, A. Okafor, T. Nwoguh, R. Sohmeshetty, Effect of Al-Si coating weights on weldability of hot-stamped ultra-high-strength steel (UsiborR 1500) used in automotive structures, Advances in Materials and Processing Technologies. (2023). https://doi.org/10.1080/2374068X.2023.2198833.

[23] D. Katundi, A. Tosun-Bayraktar, E. Bayraktar, D. Toueix, Corrosion behaviour of the welded steel sheets used in automotive industry (Tailored Welded Blanks, TWBs), in: Society for Experimental Mechanics, SEM Annual Conference and Exposition on Experimental and Applied Mechanics 2009, 2009.

[24] ISO-8407:1991-07-01, Corrosion of metals and alloys-removal of corrosion products from corrosion test specimen, International Standard. (1991).

[25] D. Mizuno, Automotive corrosion and accelerated corrosion tests for zinc coated steels, ISIJ International. (2018). https://doi.org/10.2355/isijinternational.ISIJINT-2018-159

II. EFFECT OF AL-SI COATING WEIGHTS ON WELDABILITY OF HOT-STAMPED ULTRA-HIGH-STRENGTH STEEL (USIBORR 1500) USED IN AUTOMOTIVE STRUCTURES

Hilary A. Onyishi1,2,3, Anthony C. Okafor1*, Theodore O. Nwoguh1, Raj Sohmshetty3

Department of Mechanical and Aerospace Engineering Missouri University of Science and Technology 327 Toomey Hall, Rolla, MO-65409-005, USA

Collins Aerospace: 1 Hamilton Road Windsor Locks, CT 06096, USA

Ford Research and Innovation Center 2101 Village Rd, Dearborn, MI 48124, USA

ABSTRACT

There has been increasing demand for hot-stamped pre-coated ultra-high-strength steel 22MnB5 in automotive industries for safety structures, due to its excellent properties (ultra-high strength, weight reduction, low spring back and excellent corrosion protection). This paper presents the results of experimental investigation on resistance spot welding of hot stamped Usibor 1500 to better understand the effect of aluminum-silicon (Al-Si) coating weights AS150 (150g/m^2) and AS80(80g/m^2) and welding process parameters on weldability (weld strength, weld metallurgy, weld current range, electrode wear, weld-nugget diameter, and heat treatment). The results show that the nugget diameter increases with increasing weld current, better spot-weld nugget diameter is recorded at weld currents above 7.5 kA for both AS80 and AS150 and the weld current range decreases as the interdiffusion layer (IDL) thickness increases. Heat treatment dwell time has a remarkable influence on weld current range for both AS150 and AS80 coating weights. AS80 has slightly a higher weld current range of 2.1 KA than

AS150 with weld current range of 1.8 KA. Tensile Shear Strength (TSS) for AS150 and AS80 increases nonlinearly with increase in weld diameter. Similar characteristics were observed with Cross-Tensile Strength (CTS).

1. INTRODUCTION

In the early 1900s, car and truck structures were predominantly made with wood and by the 1950s, however, automobile manufacturing industries had moved completely into using sheet steel and the industry never backed down[1]. Advanced High Strength Steel (AHSS) provides a greater opportunity for automakers to design and build stronger, stiffer, and even more-durable structures. Safety and CO_2 emission are also other challenges confronting automotive industries and have led steel makers to pursue AHSS with high impact energy absorption capacities [2]. In North America today, about 66 % of car weight structures on the road are assembled with steel. In a quest to keep the dominance of sheet metal in auto industries, the sheet metal producing industries have shifted great attention towards metal forming to reduce vehicle weight and increase strength. In today's auto industries, hot stamping has grown to become very popular in metal forming[3][4].

1.1. HOT STAMPING

Hot-stamping (also known as hot press forming) is a new technology that permits ultra-high-strength steel like carbon-manganese-boron steel alloy 22MnB5 to be formed into complex shapes, which is not feasible with cold stamping operations[5]. The

carbon-manganese-boron alloy steel 22MnB5 with Al-Si coating layer named Usibor 1500 as developed by ArcelorMittal is commonly shaped to automobile safety structures (door impact beams, bumpers, B-pillars) in the hot-stamping process. The quest by automakers to improve crashworthiness and fuel efficiency has paved the way for the increased demand for hot-stamped steel parts. Since the year 2000, there has been a rapid increase in demand for hot-stamped steel parts. By the year 2015, hot-stamped steel makers saw demand even increased higher by almost a factor of 3[6]. The manufacturing process is done in a press hardening line at this stage, the steel blank is heated to 900 °C, formed, and then quenched to room temperature. The outcome produces a hardened steel part with a yield strength of 1100 MPa and ultimate tensile strength of 1500 MPa. This can be achieved by either of the following two processes.

1.2. INDIRECT HOT-STAMPING PROCESS

In the indirect hot-stamping process, the blank is formed, trimmed, and pierced in cold conditions as shown in Figure 1. It is later heated and quenched in a die to get high strength property[7][8]. The advantages of indirect hot stamping include making parts with complex geometry, producing martensitic microstructure of the blank after complete quenching. Blanks can be pre-developed by punching, flanging, trimming, and other operations after the pre-formation to enable easier processing after it is quenched.

1.3. DIRECT HOT-STAMPING PROCESS

In the direct hot-stamping process, the blank is heated in a furnace, formed in extremely hot conditions, and then quenched in the die to produce the desired properties

as shown in Figure 2 [10][11]. Direct hot-stamping has both advantages and disadvantages.

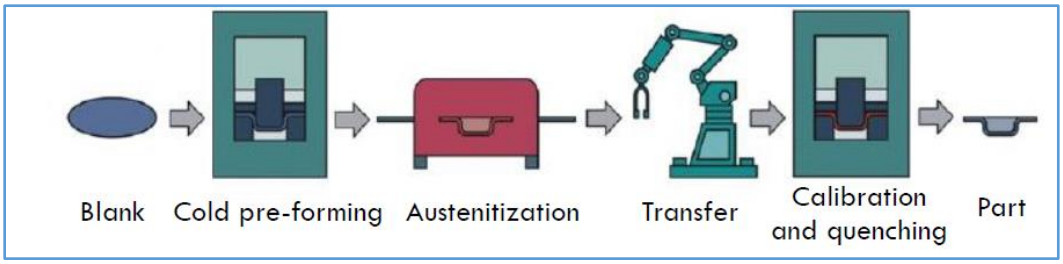

Figure 1. Indirect hot stamping (Source: Karbasian and Tekkaya 2010)[9].

The advantages include saving cost of pre-forming, accelerating production rate, and blank is flat which not only saves heating area and energy but also can be heated by a variety of heating methods, while some of the disadvantages include, it cannot be used for forming automobile parts with complex shapes, laser cutting facilities are needed and design of a cooling system for stamping dies is more complex. For instance, the direct hot forming process entails defining the entire parameters before figuring out the details of the process. Good measures are used to describe the interactions between a heated blank, cooled tool, and ambient environment. Figure 3 shows that some of the outstanding qualities of Usibor 1500 desirability in automotive industries is the ability to be used to form complex geometries with very high strength at 1500 MPa, and with no spring-back effect. There has been increased demand for hot-stamped pre-coated Usibor 1500 in automotive industries due to its excellent properties (ultra-high strength, weight reduction, low spring back and excellent corrosion protection). Usibor 1500 is a hardenable alloy of boron steel coated with Aluminum-silicon (AluSi) coating used in

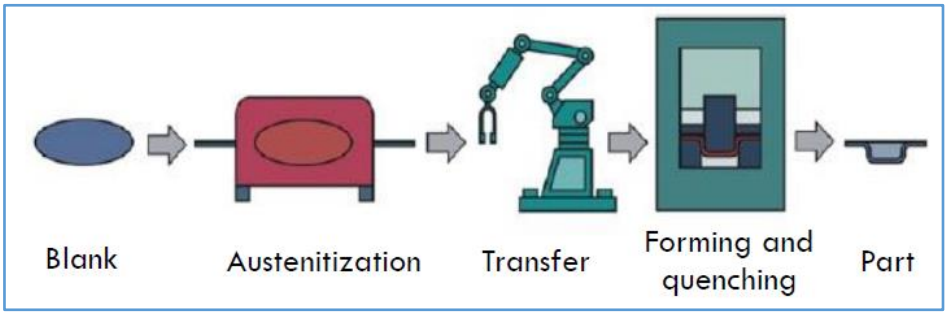

Figure 2. Direct hot-stamping (Source: Karbasian and Tekkaya 2010) [9].

automobile parts especially when high strength is desired [12]. Aluminum-silicon coating hinders steel from oxidation during heating. Allely et al [13] reported that Al and Fe oxides were made in continuous test and aluminosilicates and the combination of hydroxides after the cyclic test. It can be seen in Figure 4 that some of the outstanding qualities that made Usibor 1500 more desirable in automotive industries are its ability to be used to form complex geometries, very high strength at 1500 MPa, and with no spring-back effect. George et al [14] reported that the uniaxial tensile test specimens of Usibor 1500 were extracted and tested from the fully hardened and fully soft regions of the parts that were hot stamped at a die temperature of 400 $^{\circ}$C, the hardened section possessed fully martensitic properties with UTS of 1554 MPa. They went further to explain that in the heated (fully soft) region, the average reduction in UTS was 48 %. The differences in mechanical properties are desirable for improved crash performance of some structural components. Iman et al [15] investigated the microstructure of four different areas of the heat-affected zone (HAZ) of resistance spot welding on ultra-high strength TRIP1100 steel. Their findings showed that TRIP1100 steel microstructure contained polygonal ferrites, bainites, residual austenite (RA) and martensite/austenitic islands (M/A). They also

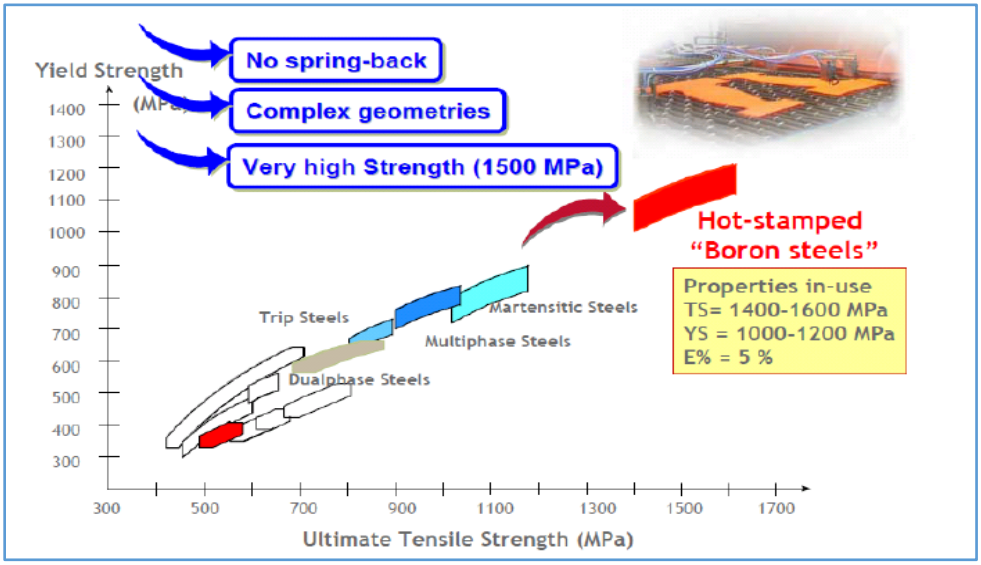

Figure 3. Main properties after hot stamping (source: Neugebauer et al. 2012) [6].

indicated that the melting (fusion) zone (FZ) has a lath martensite structure, and the grains are larger in packets. Shin and Leon [16] conducted a Parametric study in similar ultrasonic spot welding of A5052-H32 alloy sheets; their findings show that temperature measured on the weld surface provided useful information to predict if the weld quality formed by good bond density at weld interface joints was due to the combined effects of temperature rise around the horn tip and intensity of weld interface waviness. A higher weld temperature was obtained at the weld interface in the absence of a zinc layer due to the influence of sheet coupling and higher energy delivery to the workpiece [17]. Ashan et al [18] and Ashiri et al [19] reported that Liquid metal embrittlement (LME), porosity and hole-bores formations are some of the welding challenges facing welding of zinc coated automotive steels especially at medium heat conditions. Another study on spot welding of twining induced plasticity (TWIP) Steel material was carried out by Spena et

al. [20], they reported that the tensile shear strength of the welded joints increases with the increase in welding current, but the metal expulsion significantly minimizes tensile shear strength, and energy assimilation. Kim et al. [21] concluded that it is possible to obtain optimum welding conditions using Si_3N_4 tool made of the ceramic material on stir-in-plate for DP590 MPa-grade steel. An experimental study into hot-stamped boron alloy was conducted by Naderi et al. [22]. They reported that the die cooling media (water or nitrogen) have a significant effect on material properties after hot-stamping. They went further to conclude that using nitrogen as a coolant instead of water in the punch increases the yield strength by 50 to 65 MPa. Turetta et al. [23] carried another investigation on 22MnB5 formability in hot-stamping operations, they reported that in hot-stamping operations an accurate evaluation of the influence of process parameters on the properties of final sheet components is fundamental in the design and optimization of the forming process. Merklein and Lechler [24] investigated the thermal-mechanical properties of hot-stamped steel. They concluded that increasing the temperature leads to a significant decrease in flow stress values and work hardening. Ikeuchi and Yanagimoto [25] investigated the effects of hot-stamping process parameters on product properties using hot forming simulators. Their method utilized three systems for controlling the temperature history of the sheet, punch motion, and heat dissipation to the die, and permits to reproduce the hot-stamping process and to correlate the forming conditions and the properties of the formed product. On the other hands Ji et al [26] evaluated the significant impact of coating on spot-welded hot-stamped boron alloy. They reported that the contact resistance of aluminum-silicon-coated hot-stamped boron steel is lower than that of zinc-coated hot-stamped boron steel because of the thin

surface oxide layer. Cha [27] conducted investigation on welded mild steel sheet coated with aluminum. Their findings showed that the optimal welding parameters for Aluminum coated steel differ from the optimal welding parameters for uncoated steel due to the differences in the electric transmission of the coated layers. Additionally, Kyoung et al [28] reported that the Al-10%Si coating was found to promote the absorption of diffusible hydrogen at elevated temperature during hot press forming (HPF), they went further to state that the hydrogen absorbed in the aluminized press-hardened steel (PHS) was trapped mostly in the martensitic matrix, rather than in the reacted coating layer. The reacted coating layer, composed mostly of Fe-Al and Fe-Al-Si intermetallic layer, prevented the absorbed hydrogen from vaporizing through the reacted coating. The vaporization temperature of the outer aluminum-silicon intermetallic layers is higher than that of the zinc intermetallic layers. These two factors induce large changes in the heat development and weld growth mechanism at the faying surface of hot-stamped boron steels. Hot stamping is a new technology to automotive industry that provides advanced opportunity to produce automotive pre-coated ultra-high strength steels components with lighter weights and minimal spring backs. This has led many auto makers into investing lots of resources to generate wider knowledge base on hot-stamping of boron alloy that will support internal hot-stamping production. The coating thickness of AS80(80g/m^2) and AS150 (150g/m^2) have been widely accepted by automotive companies but the welding of the two-coating thickness has presented difficult challenges to the industry and solution remains unclear.

Hot stamping is relatively new technology, there have been numerous research on the technology especially with regards to its application in automotive industries

however, Usibor 1500 presents a unique challenge to automotive industries due to its desirable qualities, no research has been carried out in the past to examine the weldability of the two coating weights AS80 and AS150 of Usibor 1500. This paper presents a novel experimental investigation into the resistance spot weldability of the two coating weights AS80 and AS150 of Usibor 1500, the results will be used to validate the spot weldability performance specification and generate knowledge-based guidelines that will support internal hot stamping production of the two coating weights for Ford Motor Company and automotive applications.

2. EXPERIMENTAL SETUP AND PROCEDURES

2.1. MATERIAL PREPARATION

The experimental tests were conducted on Al-Si coated manganese-boron alloy steel 22MnB5 grade with 1.5mm gage thickness. This base metal (BM) manganese-born alloy steel is composed of low carbon steel with alloying elements of boron and manganese. The manganese-boron alloy possesses yield strength of about 400MPa, ultimate tensile strength approximately 600MPa and total elongation of 22% as it was delivered. The Al-Si coated boron alloy steel yield strength supersedes 1000MPa and ultimate tensile strength makes it to 1500 MPa with 5% total elongation after quenching process is completed hence Usibor 1500. The material gage thickness of 1.5mm with two different coating weights of AS150 (36 μm) and AS80 (20 μm) which are equivalent to AS150 (150 g/m^2) and AS80 (80 g/m^2) respectively were used. These two most common coating weights used in automobile industries were developed by

ArcelorMittal in 2013 with the rationale to (i) lower cost and (ii) introduce a coating weight that would lower the dwell time [8][12]. The chemical composition and mechanical properties of Usibor 1500 are listed in Tables 1 and 2 respectively [8][12]. The experiment is focused on determining the weldability of hot-stamped Usibor 1500 coated with two different weights of AS150 (36 μm) and AS80 (20 μm) used in automotive applications. Weldability can be defined as the ability to weld/join materials of the same or different gauge or compositions together with the use of weld guns which is imperative in building solid automotive bodies or assemblies. Table 3 shows the selected coating weights for this investigation and the applicable range of interdiffusion layers (IDL) used to prepare the two coating layers AS150 and AS80 and Table 4 shows the selected spot-welding parameters for the experiments.

Table 1. Chemical Composition of Usibor 1500

Element	C	Si	Mn	P	S	Al	Cr	Ti	B	Ni	Mo	Cu
Wt.%	0.3	0.3	1.4	0.02	0.005	0.05	0.2	0.05	0.004	0.1	0.1	0.1

Table 2. Mechanical properties of Usibor 1500

Properties	**Values**
Elongation (%)	≤ 6
Tensile Strength (MPa)	1500
Yield Strength (MPa)	1000
Microstructure	Martensite

Table 3. AS150 and AS80 Coating Designation and Thickness Requirements

Coating Designations	Condition	Total Coating Thickness (g/m^2)	Inter-diffusion Layer (IDL) Thickness (µm)
AS150	Press-hardened	150	≤16
AS80	Press-hardened	80	≤12

Table 4. Test Conditions

Machine Type	Medium Frequency Direct Control (MFDC)
Electrode Type/Face Diameter	G20-8 mm
Force	3600 N
Weld time	420 ms
Hold time	600 ms
Minimum Weld diameter	4.9 mm

The Aluminum-silicon coating on the as-received boron alloy specimen measuring about 30 µm double-sided, the mechanism of aluminum-based coating of AS150 and AS80 was achieved through interlayer diffusion process which involved pre-coating the blank of Usibor 1500. The blank was heated at an elevated temperature of 920 °C which enabled the iron diffusion to take place within 4-6minutes in the furnace, forming AlSiFe layers as shown in Figure 5. The iron diffusion was a short-monitored heating time process. Silicon composition was about 10% and 90% Aluminum. Fan and De Cooman [29] reported that it is very possible for the coating to crack, however, the cracks will get closer to the region of diffusion which makes the gage of the diffusion layer very important and must be well guarded by managing the dwell time and the

furnace temperature. Five sub-layers in Figure 4, indicated layer 1 in the as-received steel sheet were aluminum (Al) and Al-Si. The formation of microcracks could be attributed to the presence of a η-Fe2Al5 intermetallic compound in the aluminized layer which is sensitive to the thermal stress during heating and cooling[30]. The 10% silicon was added to the coating to create more elastic layers in the coating, without the inclusion of silicon, the coated layer will be very stiff and can easily be broken.

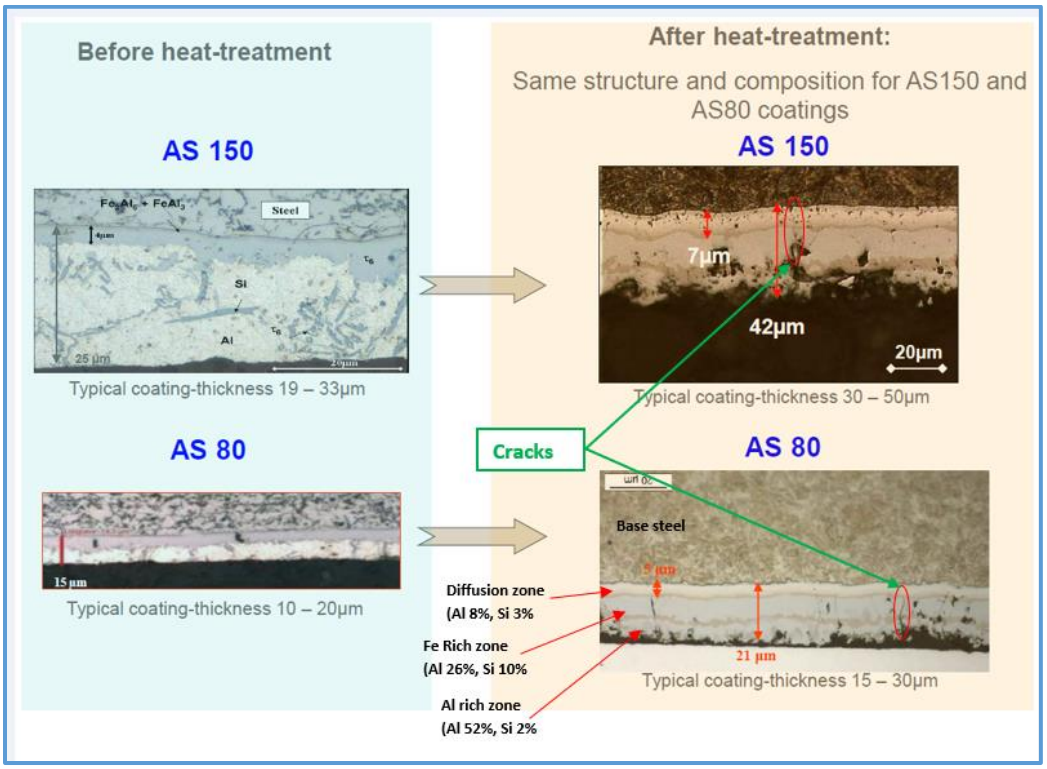

Figure 4. The Intermetallic Layers

2.2. EXPERIMENTAL WELDING PROCEDURE USING MEDIUM FREQUENCY DIRECT CONTROL MACHINE

Each sample was clamped in the spot-welding fixture shown in Figure 5 by the pneumatic pressure system. The machine was operated with a medium frequency direct control (MFDC) and an HWI 28xx EVA Inverter used for single network operation, ideal for the resistance spot-welding operation. A pneumatic pressure system was deployed to ensure optimized force during the experimental investigation process of the AS150 and AS80 samples respectively. The MFDC resistance spot-welding machine had two G20 electrodes with a 458 truncated cone designed with a diameter of 4.9 mm and chilling water in circulation. The weldability parameters under focus were weld strength, electrode wear, weld diameter, and heat treatment. These parameters were chosen based on acceptable automotive technological welding mechanisms and standards. A scanning electron microscope (SEM) was used to view the correlation between the coating layers and its weldability, especially the area where the fracture started on the tampered martensite zone to determine the maximum strength and the lower strength. After the welding processes on the samples were completed, good welds were evaluated by the weld nugget size, and the electrode life was evaluated by the number of welds per minute at a given current magnitude. The spot welding was stopped at 2000 spot welds counts without reaching the 4.9 mm minimum weld diameter at a current of 7.5 kA.

3. RESULTS AND DISCUSSIONS

3.1. WELD STRENGTH AND METALLURGY OF AS80 AND AS150 COATING WEIGHTS.

Scanning electron microscopy (SEM) was used to observe the interfacial fractures of the welds under investigation. Analysis of the microstructure of the region, at the heat-affected zone (HAZ), failure was observed when the spot weld structure had weakened in the HAZ. As can be seen in Figures 6a and 6b below, full interfacial failure was observed, as expected for AS150 in tensile shear testing and partial Interfacial failure was observed on AS80.

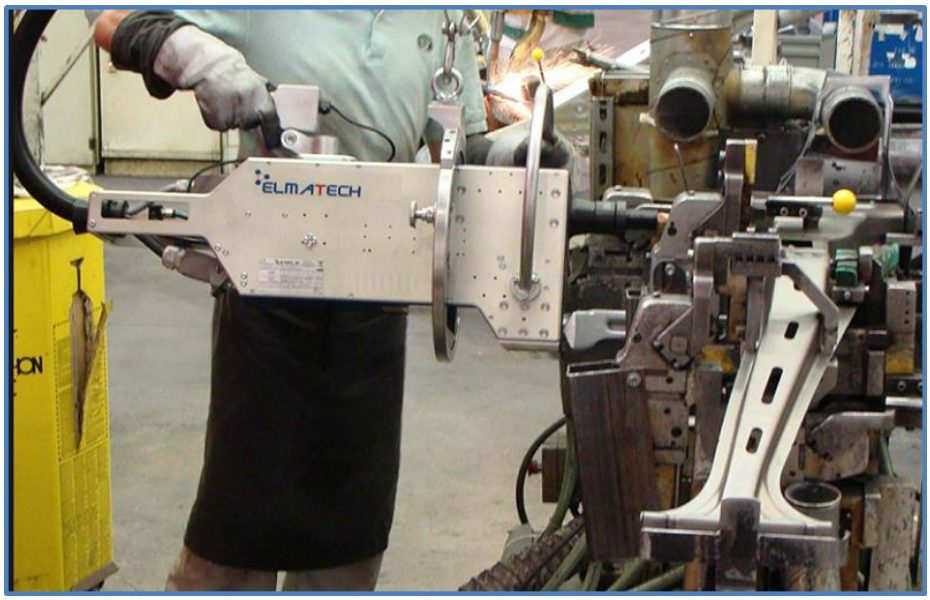

Figure 5. B-Pillar coating of AS80 and AS150 in Spot Welding Fixture.

The failure in the base metal occurs primarily when the welding process has increased weld strength higher than the base metal strength. Figure 6a shows AS150 when compared to AS80, weld nuggets close to the faying surfaces was weakly bonded and very brittle because of the molten Aluminum coating. This was monitored at the fusion zone and displayed a strong tendency to crack during loading; as a result, cracks started closer to the sharp notch at both maximum and minimum weld current. The difference between the lower and upper current is referred to as "weld current range". The detailed study of the interfacial fracture with SEM shows the fractured surface. Figure 6a shows an interfacial failure of AS150 compared to AS80 at a 2000 µm magnification. It is observed that hard cracks and reduction in sizes that were significant at the cross-sectioned nugget shown in Figure 8b were visible on the failed surface. Tensile Shear Stress (TSS) for AS150 and AS80 increases nonlinearly with increase in weld diameter from approximately 15,000 N (at weld dia. of 4.5 mm) to approximately 27,500 N (at weld dia. of 7.5mm), similar characteristic was observed with Cross-Tensile Strength (CTS). The very small features can be seen in Figure 6ci and 8cii respectively at a higher SEM magnification. This is good proof of the defects caused by the reduction in sizes and hard cracks leading to interfacial fracture that affects the spot weld properties. Figure 6a also shows that both AS150 and AS80 exhibited good spot-welding strength and metallurgy, the weld strengths were all trending above 4.9mm minimum weld diameter threshold which is a good indication that AS150 and AS80 can be spot welded at desirable weld strengths applicable in automotive industries under minimum weld current range of 2.1kA for AS80 and 1.8kA for AS150 as shown in figure 6d.

The hardness distribution of the weld is shown in Figure 7, when AS150 is welded to another AS150 or AS80 welded to another AS80, the weakest area in the assembly turns out to be the heat-affected zone (HAZ). As can be seen, Usibor 1500 which is the base materials hardness would be approximately 500 HV constant hardness, however, the hardness in the weld zone was trending within 350 HV for the two selected coating weights.

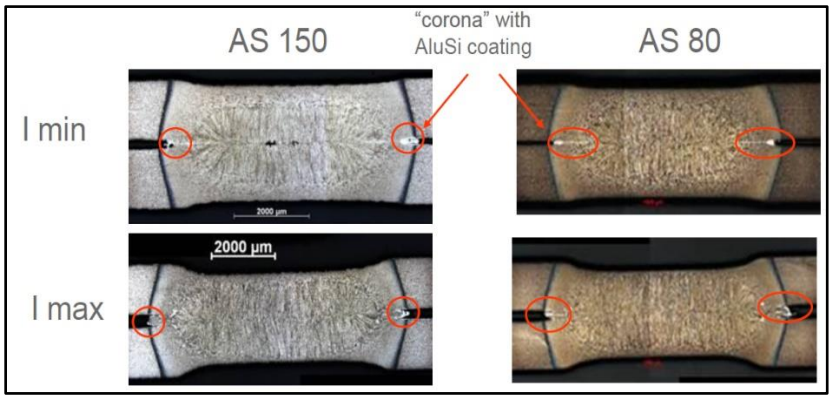

(a)

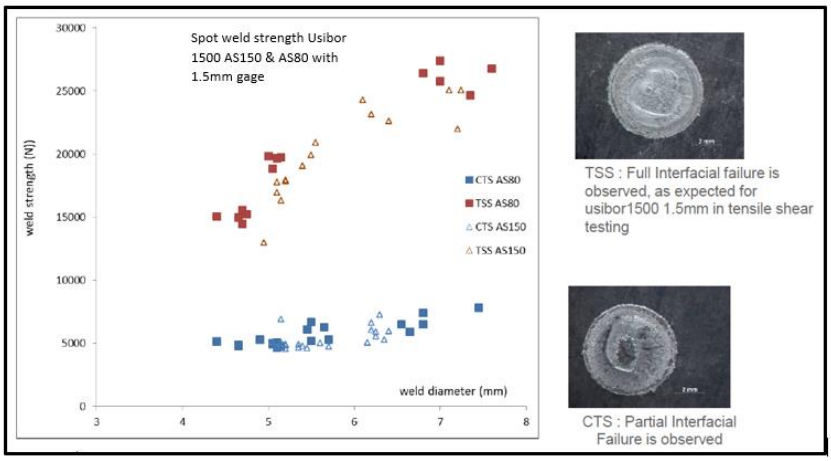

(b)

Figure 6. (a) AS150 and AS80 Weld Metallurgy. (b) Figure 6b. Tensile Strength vs weld diameter. (c) Evaluation of Tensile Shear Stress (TSS) and Cross-Tensile Strength (CTS). (d) Comparison of AS80 and AS150 weld current range.

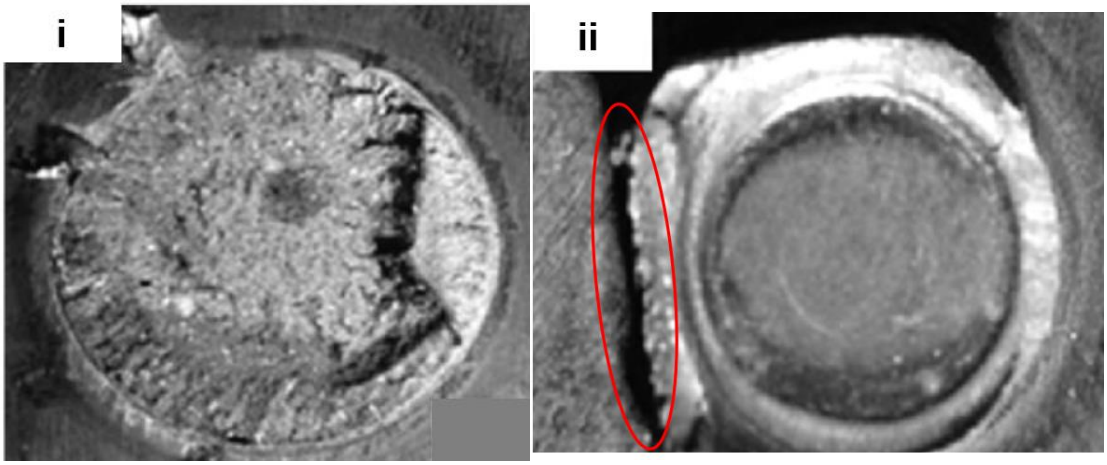

(c)

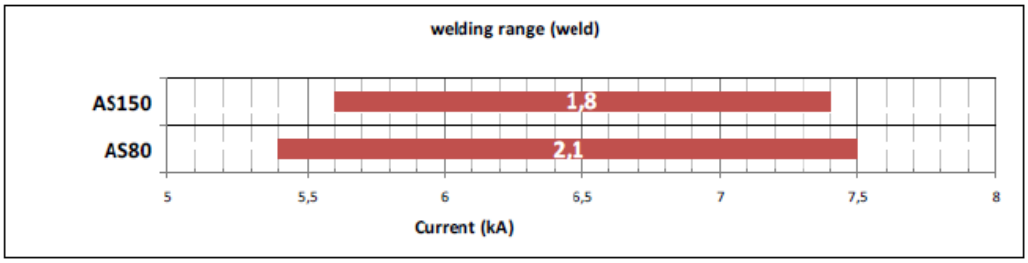

(d)

Figure 6. (a) AS150 and AS80 Weld Metallurgy. (b) Figure 6b. Tensile Strength vs weld diameter. (c) Evaluation of Tensile Shear Stress (TSS) and Cross-Tensile Strength (CTS). (d) Comparison of AS80 and AS150 weld current range (cont.).

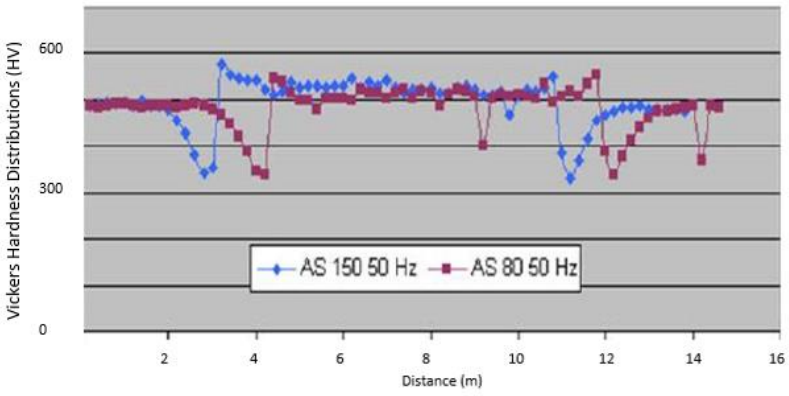

Figure 7. Vickers Hardness Distribution of AS150 and AS8.

3.2. INFLUENCE OF THE HEAT TREATMENT ON WELDABILITY OF AS80 AND AS150 COATING WEIGHTS

The minimum welding current (I_{min}) which is the welding current required to produce a minimum weld spot (nugget) diameter ($d\text{-}_{wmin} = 4\sqrt{t}$, where t is the sheet thickness) for this experiment was determined and set by the weld nugget diameter of 4.9 mm which can be seen in Figure 8 as the lower shear strength of the weld. The maximum welding current (I_{max}) is determined as the current that caused the expulsion of liquid metal from the weld specimen interface. Expulsion could be clarified as those spot-welding defects emanating from the molten metal ejected from the base metals. The welding current range (ΔI) is defined as the difference between the minimum welding current and the maximum welding current. It could be seen that good weld current ranges were obtained measuring from 2.3 kA, 1.8 kA, and the lowest at 0.8 kA as a function of heat treatment dwell time at 5.5-, 7.5- and 9-min dwell times respectively for each experiment carried out on AS150 and AS80. It is established here that heat treatment influences weldability range on AS150, and similar phenomena are observed on AS80.

The heat treatment has a remarkable influence on the welding range of both AS150 and AS80 coating weights. This is made possible because of the kind of alloy layer resulting from hot stamping. The Interdiffusion layer (IDL) is the ability of the coating weights to mix homogenously with the base metal (Usibor 1500) indicated in Figures 9 and 10.

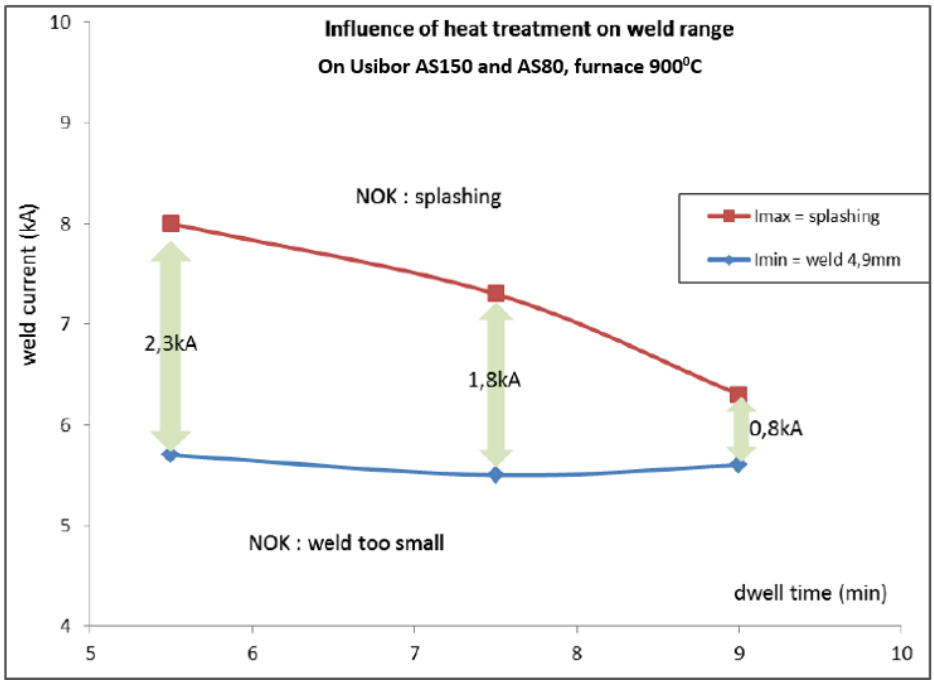

Figure 8. Influence of heat treatment on weldability of AS150 and AS80.

The two figures show that the weld current range decreases as the interdiffusion layer (IDL) thickness and overall coating thickness increases though AS80 coating develops “faster” than AS150.

3.3. ELECTRODE WEAR PERFORMANCE ON AS80 AND AS150 COATING WEIGHTS

Figures 11a and b show the results for electrode wear test for USIBOR 1500 with AS150 and AS80 coating weight respectively. The electrode wear performance was evaluated by subjecting the two Al-Si-coating thickness to the same weld conditions. The objective was to understand which coating weight will give a longer electrode life better than the other. Figures 11a and 11b look exactly alike because no significant difference was noted among the two coating weights.

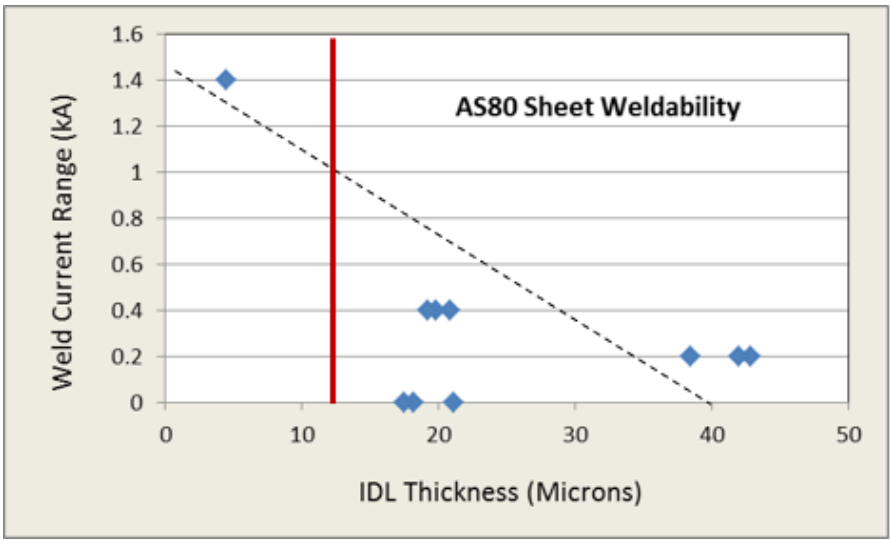

Figure 9. Weld current effect on AS80 coating thickness.

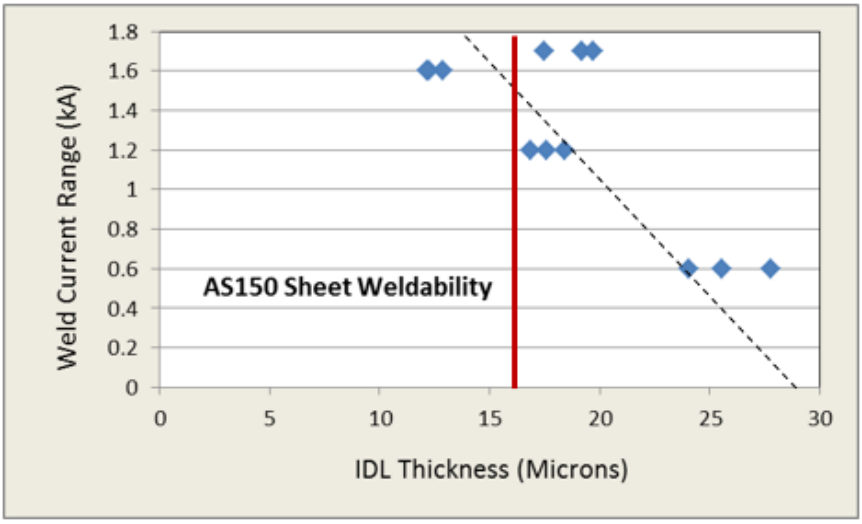

Figure 10. Weld current effect on AS150 coating thickness.

The green line at 4.9 mm minimum weld nugget diameter mark indicates that for both coating weights AS80 and AS150, 2000 good spot welds were obtained on each coupon of AS80 and AS150 with all weld nugget diameters measuring above 4.9 mm defined as the minimum weld diameter for the investigated resistance spot welding and

is acceptable for automotive industry applications. A good weld is evaluated by the weld nugget size formation, and the electrode life is evaluated by the number of welds per minute at a given current magnitude. The spot welding was stopped at 2000 spot welds counts without reaching the 4.9 mm minimum weld nugget diameter at a maximum current of 7.5 kA. This indicates long electrode life has been observed as well, and the coating weight has no influence on the electrode performance. Figure 12 shows a sample of the coupon cut out displaying good spot-welds were achieved during the investigations process.

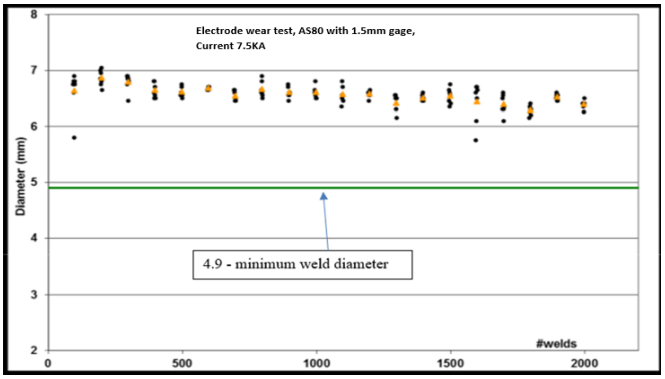

(a)

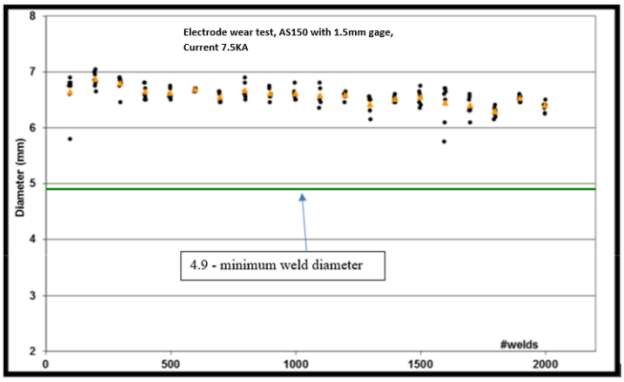

(b)

Figure11. (a) Electrode Wear: Weld Diameter Vs Number ofWelds on AS150. (b) Electrode Wear: Weld Diameter Vs Numberof Welds on AS80.

Figure. 12 Sample of Spot Weld counts.

4. CONCLUSION

4.1. CONCLUSION AND FUTURE WORK

This research studied the effect of different coating weights (AS80 and AS150) on weldability of hot-stamped Usibor 1500 used in high-strength automotive structural components to further understand which material would perform better for automotive application. The following conclusions can be made from the investigation:

Successful spot welding operations can be carried out to marry a stack up of 1.5 mm gauges of USIBOR 1500 with coating weights of AS80 and AS150 as both coating weights exhibited good spot-weld nugget diameter and metallurgy, the weld nugget diameter were all trending above 4.9 mm minimum weld nugget diameter which is most suitable for automotive industry application, and a good indication that AS150 and AS80 can be spot-welded to produce a desirable weld strength for either AS80 or AS150 stack up as may be applicable in automotive industries.

Tensile Shear Strength (TSS) for AS150 and AS80 increases nonlinearly with increase in weld diameter from approximately 15,000 N (at weld nugget dia. of 4.5 mm) to approximately 27,500 N (at weld nugget dia. of 7.5mm), similar characteristic was observed with Cross-Tensile Strength (CTS). Both AS150 and AS80 exhibited good spot-welding strength and metallurgy, the weld strengths were all trending above 4.9mm minimum weld diameter threshold which is a good indication that AS150 and AS80 can be spot welded at desirable weld strengths applicable in automotive industries under minimum weld current range of 2.1kA for AS80 and 1.8kA for AS150.

2000 good spot welds were obtained on each coupon with AS80 and AS150 coating weights, before the spot welding was terminated, as all weld nugget diameters were above 4.9 mm defined as the minimum weld diameter for the investigated resistance spot welding and is acceptable for automotive industry applications.

Nugget diameter (electrode life) at welding current of 7.5 KA decreases gradually with increasing spot weld count, from nugget diameter of about 7 mm initially, which is above the 4.9 mm minimum weld nugget diameter, to a nugget diameter about 6.5 mm at 2000 spot weld count for both AS150 and AS80 coating weights.

There is no significant influence of the coating thickness on the electrode life, the coating weight does not influence the weld strength, nor the welding metallurgy of both AS150 and AS80 though AS80 has a slightly better performance. Heat treatment dwell time has a remarkable influence on weld current range for both AS150 and AS80 coating weights. AS80 has slightly a higher weld current range of 2.1 KA than AS150 with weld current range of 1.8 KA. The weld current range decreases as the interdiffusion layer (IDL) thickness and overall coating thickness increases, but in terms

of coating development, AS80 coating develops “faster” than AS150 apparently because of lesser coating thickness. Weld nugget diameter increases with increasing weld current and better spot-weld nugget diameter is recorded at weld currents above 7.5 kA for both AS80 and AS150 coating weight; But weld nugget diameter decreases slightly for both AS80 and AS150 at weld currents above 8.5 kA primarily because of expulsion at the faying surface.

4.2. FUTURE WORK

Coupled with cost reduction opportunities, further research work should be carried out to study the feasibility of spot welding a stack up of AS80 and AS80 with 1.5mm and 1mm gage to avoid unexpected production or parts performance issues. Also, corrosion studies of resistance spot welded joints of USIBOR 150 with AS80 and AS150 coatings to ascertain their corrosion resistance, types, and mechanism.

REFERENCES

[1] POSCO Co. LTD. posco automotive steel data book. 2008.

[2] Ashiri R, Marashi SPH, Park YD. Weld Processing and Mechanical Responses of 1-GPa TRIP Steel Resistance Spot Welds. Welding Journal 2018;97:157S-169S. https://doi.org/10.29391/2018.97.014.

[3] Huang MD, Wang BY, Zhou J. Hot Stamping Parameters Optimization of Boron Steel Using a Response Surface Methodology Based on Central Composite Design. Journal of Iron and Steel Research International 2015. https://doi.org/10.1016/S1006-706X(15)30035-2.

[4] Billur E, Altan PDT. Challenges in Forming Advanced High Strength Steels. New Developments in Sheet Metal Forming 2010:285–304.

[5] Altan T, Groseclose A, Billur E, Subramonian S, Mao T. Advances and challenges in sheet metal forming technology 2013:1–6.

[6] Neugebauer R, Schieck F, Polster S, Mosel A, Rautenstrauch A, Schönherr J, et al. Press hardening - An innovative and challenging technology. Archives of Civil and Mechanical Engineering 2012. https://doi.org/10.1016/j.acme.2012.04.013.

[7] Engels, H., Schalmin, O. and Muller-Bollenhagen C. Controlling and monitoring of the hot-stamping process of boron-alloyed heat-treated steels. Proc. Int. Conf. "New Development in Sheet Metal Forming Technology, 2006, p. 135–150.

[8] Billur E, Wang C, Bloor C, Holecek M, Porzner H, Altan T. Advancements in tailored hot stamping simulations: Cooling channel and distortion analyses, 2014. https://doi.org/10.1063/1.4850158.

[9] Karbasian H, Tekkaya AE. A review on hot stamping. Journal of Materials Processing Technology 2010. https://doi.org/10.1016/j.jmatprotec.2010.07.019.

[10] Billur E, Wang C, Bloor C, Holecek M, Porzner H, Altan T. Advancements in tailored hot stamping simulations: Cooling channel and distortion analyses, 2014. https://doi.org/10.1063/1.4850158.

[11] Li Y, Tan N, Xu Z, Luo Z, Han K, Zhai Q, et al. Enhancement of fatigue endurance by Al-Si coating in hot-stamping boron steel sheet. Metals 2019. https://doi.org/10.3390/met9070722.

[12] Hot Stamping of Ultra High-Strength Steels. 2019. https://doi.org/10.1007/978-3-319-98870-2.

[13] Allély C, Dosdat L, Clauzeau O, Ogle K, Volovitch P. Anticorrosion mechanisms of aluminized steel for hot stamping. Surface and Coatings Technology 2014. https://doi.org/10.1016/j.surfcoat.2013.10.072.

[14] George R, Bardelcik A, Worswick MJ. Hot forming of boron steels using heated and cooled tooling for tailored properties. Journal of Materials Processing Technology 2012. https://doi.org/10.1016/j.jmatprotec.2012.06.028.

[15] Hajiannia I, Shamanian M, Atapour M, Ghassemali E, Ashiri R. A microstructure evaluation of different areas of resistance spot welding on ultra-high strength TRIP1100 steel. Cogent Engineering 2018;5:1–13. https://doi.org/10.1080/23311916.2018.1512939.

[16] Shin HS, De Leon M. Parametric study in similar ultrasonic spot welding of A5052-H32 alloy sheets. Journal of Materials Processing Technology 2015. https://doi.org/10.1016/j.jmatprotec.2015.05.013.

[17] Haddadi F, Abu-Farha F. Microstructural and mechanical performance of aluminium to steel high power ultrasonic spot welding. Journal of Materials Processing Technology 2015. https://doi.org/10.1016/j.jmatprotec.2015.06.019.

[18] Ahsan MRU, Kim YR, Kim CH, Kim JW, Ashiri R, Park YD. Porosity formation mechanisms in cold metal transfer (CMT) gas metal arc welding (GMAW) of zinc coated steels. Science and Technology of Welding and Joining 2016;21:209–15. https://doi.org/10.1179/1362171815Y.0000000084.

[19] Ashiri R, Haque M, Ji C, Shamanian M, Salimijazi H, Park Y-D. Supercritical area and critical nugget diameter for liquid metal embrittlement of Zn-coated twining induced plasticity steels. Scripta Materialia 2015;109:6–10. https://doi.org/10.1016/j.scriptamat.2015.07.006.

[20] Russo Spena P, De Maddis M, Lombardi F, Rossini M. Investigation on Resistance Spot Welding of TWIP Steel Sheets. Steel Research International 2015. https://doi.org/10.1002/srin.201400336.

[21] Kim YG, Kim JS, Kim IJ. Effect of process parameters on optimum welding condition of DP590 steel by friction stir welding. Journal of Mechanical Science and Technology 2014. https://doi.org/10.1007/s12206-014-1138-7.

[22] Naderi M, Uthaisangsuk V, Prahl U, Bleck W. A Numerical and Experimental Investigation into Hot Stamping of Boron Alloyed Heat-Treated Steels. Steel Research International 2008. https://doi.org/10.1002/srin.200806320.

[23] Turetta A, Bruschi S, Ghiotti A. Investigation of 22MnB5 formability in hot stamping operations. Journal of Materials Processing Technology 2006. https://doi.org/10.1016/j.jmatprotec.2006.04.041.

[24] Merklein M, Lechler J. Investigation of the thermo-mechanical properties of hot stamping steels. Journal of Materials Processing Technology 2006. https://doi.org/10.1016/j.jmatprotec.2006.03.233.

[25] Ikeuchi K, Yanagimoto J. Valuation method for effects of hot stamping process parameters on product properties using hot forming simulator. Journal of Materials Processing Technology 2011. https://doi.org/10.1016/j.jmatprotec.2011.03.017.

[26] Ji CW, Jo I, Lee H, Choi ID, do Kim Y, Park Y Do. Effects of surface coating on weld growth of resistance spot-welded hot-stamped boron steels. Journal of Mechanical Science and Technology 2014. https://doi.org/10.1007/s12206-014-1043-0.

[27] J. H. Cha. A study on resistance spot weldability of aluminum coated sheet steels. Pukyong National University, 2002.

[28] Jo KR, Cho L, Sulistiyo DH, Seo EJ, Kim SW, De Cooman BC. Effects of Al-Si coating and Zn coating on the hydrogen uptake and embrittlement of ultra-high strength press-hardened steel. Surface and Coatings Technology 2019. https://doi.org/10.1016/j.surfcoat.2019.06.047.

[29] Fan DW, De Cooman BC. State-of-the-knowledge on coating systems for hot stamped parts. Steel Research International 2012. https://doi.org/10.1002/srin.201100292.

[30] Suehiro M, Kusumi K, Miyakoshi T, Maki J, Ohgami M. Properties of aluminum-coated steels for hot-forming. Nippon Steel Technical Report 2003.

III. ENHANCEMENT OF VISCOSITY AND THERMAL CONDUCTIVITY OF SOYBEAN VEGETABLE OIL USING NANOPARTICLES TO FORM NANOFLUIDS FOR MINIMUM QUANTITY LUBRICATION MACHINING OF DIFFICULT-TO-CUT METALS

Hilary A. Onyishi1,2,3, Anthony C. Okafor1*, Theodore O. Nwoguh1

Department of Mechanical and Aerospace Engineering Missouri University of Science and Technology 327 Toomey Hall, Rolla, MO-65409-005, USA

Collins Aerospace: 1 Hamilton Road Windsor Locks, CT 06096, USA

Ford Research and Innovation Center 2101 Village Rd, Dearborn, MI 48124, USA

ABSTRACT

Sustainable use of vegetable oil as a base fluid in minimum quantity lubrication (MQL) strategy for machining advanced materials is promising but limited due to their low thermal conductivity and viscosity. This paper presents the results of experimental investigation for enhancing viscosity and thermal conductivity of high oleic soybean vegetable oil (HOSO) using Al2O3, MoS2, and TiO2 nanoparticles (30 nm particle size and 0.5–4.0% wt. concentration) inclusion to form nanofluids at a temperature ranging from 25 to 70 °C for use in vegetable oil-based nanofluids-MQL machining of difficult-to-cut metals. The result shows that the viscosity and thermal conductivity of HOSO increases with an increase in nanoparticle weight concentration, but there is a decrease in the suspension stability of the nanofluid. Also, the viscosity of HOSO nanofluids decreases with an increase in temperature, but thermal conductivity increases with an increase in temperature, while for the base HOSO, it decreases with an increase in temperature. This is a very significant positive observation especially for difficult-to-cut

materials that generate high heat that need to be conducted away from the cutting zone. Thermal conductivity and viscosity were enhanced up to 55% (using MoS2 at 70 °C and 4% wt. 98 concentration) and 11.5% (using TiO2 at 50 °C and 3.5% wt. concentration), respectively. The Brownian motion of the nanoparticles and liquid-solid interlayer interfaces are responsible for this behavior of the nanofluid thermal conductivity, while nanoparticle thickening and entangle mechanisms were responsible for the behavior of the nanofluid viscosity. This implies that a lower oil flow rate can be applied during machining of Inconel-718 due to increased viscosity and thermal conductivity to obtain optimal machining performance, lower power consumption, and reduce the negative impact on the environment.

1. INTRODUCTION

Materials researchers are always looking for means to provide tougher materials used in engineering applications. These advanced materials need to be machined to their desired shape for specific applications. Cutting tools used during machining experience increased heat due to high friction and cutting forces generated at the cutting zone causing thermal softening of the cutting tool material, rapid tool wear, and shorter tool life. These adverse effects on the cutting tools also lead to reduced performance of the machined part due to reduced surface integrity such as high residual stresses and poor surface finish. Cutting fluids are used to improve surface integrity. The cutting fluid acts as a lubricant to reduce friction and as a coolant to cool the temperature at the cutting zone. Environmentally unfriendly conventional emulsion coolant (CEC) is the most

effective cutting fluid for machining advanced materials like Inconel-718, titanium alloy, and compacted iron graphite used in aerospace, nuclear, and automotive industries. The viscosity and thermal conductivity of fluids used in these applications are of utmost importance to researchers and manufacturers and determine the suitability of the cutting fluid. Theoretical models have been proposed for determining these intrinsic properties, but these properties are best obtained by experimental investigation [1–3] due to the limitation of available models.

Nanofluids have been proposed to be an effective medium for transferring heat in applications such as heat exchangers, solar energy, and geothermal energy. Nanofluid is the suspension of nanoparticles in a base fluid to improve the thermal conductivity of the base fluid. The base fluid predominantly reported in the literature is water, but vegetable oil is attracting a lot of interest due to its advantages over water. The nanoparticles could be metallic or non-metallic, and the nanofluid so formed could be conventional nanofluid (single type of nanoparticle of the same average size) or hybrid nanofluid (multi-type of nanoparticles of same or different average sizes). Pryazhnikov et al. [4] studied thermal conductivity of nanofluids using different volumes up to 8%concentrations of SiO2, Al2O3, TiO2, ZrO2, and CuO and diamond nanoparticles of varying sizes up to 150 nm at room temperature and using water, ethylene glycol, and engine oil as base fluids. After comparing their results with existing models, they concluded that the thermal conductivity coefficient at room temperature is dependent on nanoparticle volume percentage, size, and property of the base fluid. Asadi et al. [5] studied the effect of adding hybrid nanoparticles (MgO-MWCNT) to engine oil to form nanofluid. They showed that by increasing hybrid nanoparticle mass concentration to

2% and increasing temperature to 50 °C, thermal conductivity can be enhanced by 65%. Omrani et al. [6] studied thermal conductivity and viscosity of multi-walled carbon nanotubes with different length and outer diameter sizes using a volume fraction of 0.05% and deionized water as base fluid. The result showed an enhancement of 36% and 5.5% in the thermal conductivity and viscosity, respectively. Chandrasekar et al. [7] investigated the thermal conductivity and viscosity of aluminum oxide/water nanofluid using 43 nm nanoparticle size at room temperature experimentally and theoretically. Nanofluid at different volume percentages was prepared using a microwave-assisted chemical precipitation method and dispersion using a sonicator. It was observed that thermal conductivity and viscosity increased with volume concentration. Turgut et al. [8] investigated the effect of TiO2 nanoparticles with deionized water as base fluid on thermal conductivity and viscosity measurement of the formed nanofluid. The result showed an increase in thermal conductivity of 7.4% at a volume concentration of 3% at a temperature of 13 °C. They also observed that the increase in viscosity was higher than that predicted using the Einstein model. Vajjha and Das [9] experimentally investigated the thermal conductivity of aluminum oxide, copper oxide, and zinc oxide nanofluids using ethylene glycol and water mixture ratio 60:40 as base fluid. They also compared their results with those obtained using various existing models and observed that the results do not exhibit good agreement. Corcione [10] showed that effective thermal conductivity and dynamic viscosity of nanofluids are dependent on the size of the nanoparticle, base fluid, volume fraction of the nanoparticle, and application temperature. These factors make it very difficult to use existing viscosity and thermal

conductivity models to theoretically determine the effective thermal conductivity and viscosity of different nanofluids.

usually from 300 to 3000 l/h to the cutting zone, which provides the necessary lubrication and transfer of heat away from the cutting zone when machining, especially difficult-to-cut materials [11]. The frequent use of emulsion coolant has an adverse effect on the environment, machine operators, and the economy. Mineral resources are non-renewable, proper disposal of used emulsion coolant is difficult and very expensive, and machining operators with respiratory and skin diseases have been known to be associated with constant exposure to mineral oil-based emulsion cutting fluids. The application of nanofluid in machining using emulsion coolant as base fluid is not feasible due to the large amount of fluid that is needed, the filtration system used during emulsion coolant application, and suppling the nanoparticle to the cutting zone will not be sustainable. Chetan et al. [12] investigated the application of alumina powder, colloidal solution of silver, and sunflower oil in water for use as nanofluid in the turning process. They observed that nanoparticles affect the contact angle, surface tension, droplet size, and spreadability of the fluid which also reduce tool wear and cutting forces. The present need for sustainable, renewable, biodegradable, and environmentally friendly cutting fluids has been at the forefront of research in machining for decades. The use of vegetable oil has found its niche in machining materials such as mild steel and aluminum alloys in the form of minimum quantity lubrication (MQL).

MQL is the application of a small amount of oil supplied to the cutting zone with the aid of pressurized air to form atomized molecules of oil in the air. In MQL machining, the air pressure breaks a precise amount of oil into droplets. The aerosol

applied to the cutting zone via a nozzle forms a lubricating film, inhibits friction and heat growth, and flushes the chips away from the cutting zone. These methods have been very effective in machining soft materials like mild steel and aluminum alloys. In cutting difficult-to-cut metals, problems are still experienced due to a large amount of heat generated when machining materials like Inconel 718, compacted graphite iron, and titanium alloy. Recent studies have tried to solve such problems using cryogenic MQL [13–15], the application of cryogenic fluid in combination with MQL, or replacing pressurized shop air with chilled air. These procedures are associated with the hardening of the materials and further increase cutting forces and tool breakage due to sudden cooling. Sidik et al. [16] conducted a review of the nanofluid application in MQL, and it was observed that most application has been on soft materials like steel, aluminum, and pure titanium; the base fluid has been deionized water, ethyl-glycol, and ester oil. Behera et al. [17] investigated the spreadability of metalworking fluid using aluminum oxide and different surfactants in deionized water during turning. The improvement in machinability was observed to be due to the spreadability of the nanofluid. Yuan et al. [18] investigated the influence of copper, silicon carbide, and diamond nanoparticles in different vegetable oil for use as nanofluid in end-milling of aluminum alloy using MQL application. It was observed that the nanofluid shows an improvement compared to dry machining by lowering cutting force and surface roughness. Li et al. [19] investigated the influence of graphene oxide nanofluid (graphene oxide suspended in commercially available synthetic ROCOL oil) on cutting temperature in machining Ti6Al4V. The result showed that the addition of nanoparticles reduced the cutting temperature and friction force.

Vegetable oils comprise mainly fatty acids that are either saturated or unsaturated. Saturated fatty acids have higher melting temperatures and most times solid at room temperature, while unsaturated fatty acids have low melting temperatures and tend to be liquid at room temperature. The viscosity and thermal conductivity of fluids used as the load-carrying fluid in moving parts and cooling medium in thermal applications are very important properties of the fluid. During machining of difficult-to-cut materials, the fluid in the cutting zone is subjected to shear stress and heat deformation due to shearing during chip formation. Viscosity and thermal conductivity of fluids are dependent on the shear rate and temperature. When machine difficult-to-cut metals such as Inconel-718, lower cutting speeds are used, and high cutting temperatures are generated compared to the not difficult-to-cut metals such as aluminum and steel. In MQL machining, the pressure and flow rate are very low compared to conventional emulsion flood cooling, therefore, the need to supply fluids with enhanced viscosity without inhibiting the fluidity of the fluid. A recent study shows that increasing oleic (unsaturated) fatty acids composition in soybean, vegetable oil can enhance the viscosity of soybean oil but not the thermal conductivity [20]. From the above literature reviewed, knowledge of the effect of nanoparticles on intrinsic properties of vegetable oil for use in machining difficult-to-cut metal is lacking and needs to be investigated. To enhance the thermal conductivity of base vegetable oil for use in machining and understand its properties, AlO3, TiO2, and MoS2 nanoparticles of 30 nm nanoparticle size were added and uniformly suspended in high oleic soybean oil (HOSO) to form AlO3/HOSO-, TiO2/HOSO-, and MoS2/HOSO nanofluids to investigate the effect of type of nanoparticle of the same nanoparticle size, weight concentration, temperature on shear

stability, suspension stability, viscosity, and thermal conductivity before their application in MQL machining of difficult-to-cut metals. Nanofluid-MQL or minimum quantity nano-lubrication is the application of MQL with nanoparticles in the base fluid. High oleic soybean oil has been shown to have the potential to replace mineral oil-based conventional emulsion flood coolant as a cutting fluid in the form of MQL application [21]. Modifying the fatty acid content of soybean oil is one method of increasing the viscosity of soybean oil. The method involves reducing the saturated fatty acid and polyunsaturated fatty acid contents which are solid at room temperature and have a high oxidation rate, respectively. The method increases viscosity, oxidation stability, and shear stability without inhibiting the fluidity of the fluid. The influence of nanoparticles on rheological properties of nanofluid (viscosity and thermal conductivity) using high oleic soybean oil (HOSO) as the base fluid has never been investigated, and most of the nanofluid studies reported in the literature used water, engine oil, or ethyl glycol as base fluids in other applications such as heat transfer fluids, most of which are limited to room temperature.

This study investigated the influence of three types of nanoparticles (titanium oxide (TiO2), molybdenum disulfide (MoS2), and aluminum oxide (Al2O3)), varying nanoparticle weight concentration from 0.5 to 4%wt., and temperature range (25 to 70 °C) on shear stress, viscosity, thermal conductivity, and suspension stability of HOSO using the same 30 nm nanoparticle size in high oleic soybean vegetable oil as the base fluid for potential use in nanofluids minimum quantity lubrication (nMQL) machining of difficult-to-cut materials.

2. MATERIALS AND METHOD

2.1. PREPARATION OF NANOFLUIDS

High oleic soybean vegetable oil (HOSO) was selected as a base fluid for comparative evaluation of three nanofluids based on our recent comparative study of high oleic soybean oil (HOSO), low oleic soybean oil (LOSO), Acculube 2000, and conventional emulsion flood coolant (CEFC) that showed the outstanding performance and potential of HOSO as cutting fluid for machining Inconel 718 using minimum quantity lubrication. Titanium oxide (TiO2), molybdenum disulfide (MoS2), and aluminum oxide (Al2O3) nanoparticles were selected based on extensive literature review due to their compatibility with difficult-to-cut metals like Inconel-718 and their insolubility in the base vegetable oil. Uniform average nanoparticle size of 30 nm was selected based on the reported data in the literature on the effect of nanoparticle size that shows improvement in rheological properties of nanofluids with the decrease in particle size, and 30 nm is the lowest nanoparticle size that can be obtained across all nanoparticles investigated from nanoparticle manufacturers. The nanoparticle size of 30 nm was kept constant for all three nanoparticles to eliminate the influence of nanoparticle size on the result of the experiments. High oleic soybean oil was supplied by Archer Daniels Midland, USA. The nanoparticles used in the study were purchased from NANOSHEL, in the UK.

The varying weight percentage of nanoparticles from 0.5, 1, 1.5, 2.0, 2.5, 3.0, 3.5, and 4.0% and high oleic soybean oil were weighed using Torbal analytical balance with 0.0001 g accuracy. Each high oleic soybean oil with a measured weight percentage

of nanoparticle was mixed mechanically and placed inside an ultrasonic bath for 2 h to disrupt the attraction between similar matter (liquid and solid) and further enhance the solid-liquid mixture. After sonication, the mixture is mechanically mixed once again before each test is carried out.

2.2. SHEAR STRESS-SHEAR RATE AND VISCOSITY TEST

DHR II Rheometer from the TA instrument was used to conduct the viscosity and shear stress-shear rate experiments on the HOSO base fluid and the nanofluids as shown in Figure 1. The DHR II was calibrated before each experiment using XHATCH – 40 mm parallel plate and Peltier plate. The experiments were conducted only after the calibration inertia, geometry inertia, friction, and gap temperature were within manufacturers' recommendation using a 700 μm gap and 35 μm trim gap offset (5%of the gap) to ensure proper loading and correct filling of the sample. The shear rate range was selected based on a preliminary test with HOSO base fluid using 0 to 100 1/s shear rate range. The temperature of the HOSO base fluid and nanofluid for each test was set using the environment control temperature for DHR II from25 to 70 °C. For each shear rate, the corresponding shear stress is obtained. The shear stress versus shear rate data was plotted, and the plots were then used to obtain the viscosity for the nanofluids and base fluid for a Newtonian fluid [20].

2.3. THERMAL CONDUCTIVITY TEST

Thermal conductivity tests of the HOSO base fluid and nanofluids were conducted using a Thermtest TLS-100 portable thermal conductivity meter with ASTM

and IEEE standards [20]. The transient line source meter uses a 100-mm needle sensor consisting of a thin heating wire and temperature sensor.

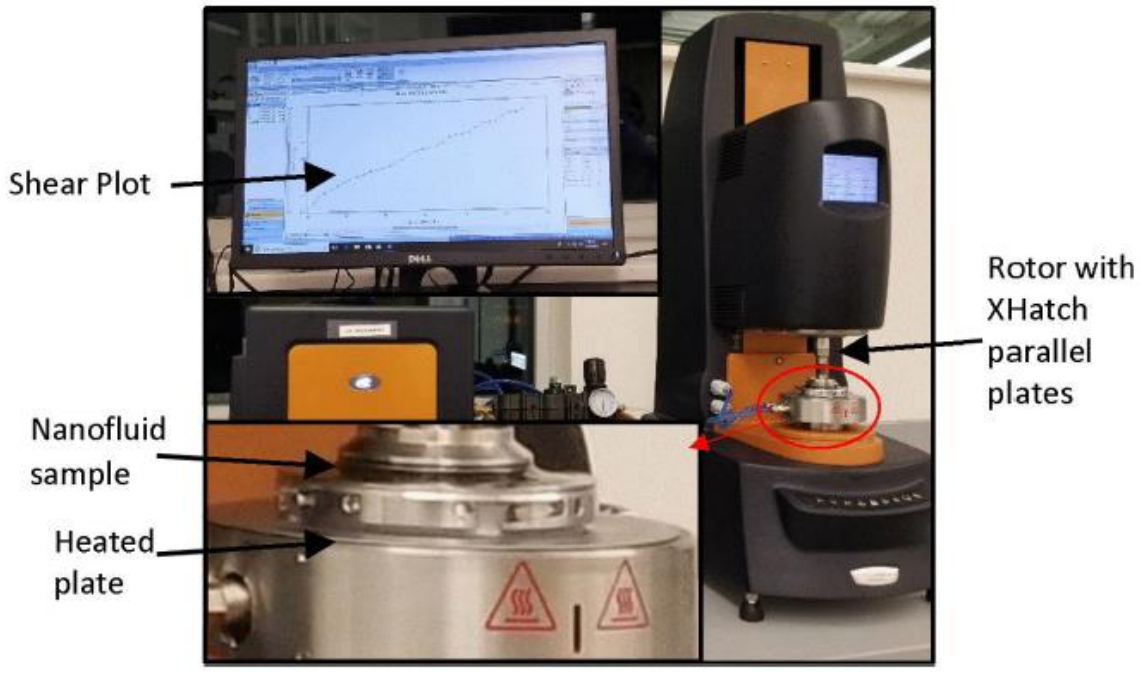

Figure 1. Photograph of the experimental setup for rheology study using DHR-II.

The sensor was completely inserted into the sample tube placed in a water bath for varying temperature ranges from 25 to 70 °C; water bath heater was set to measurement temperature and allowed to stabilize; aluminum foils were used to control evaporation and cooling of the samples during thermal conductivity measurement, and experiments were conducted only when TLS-100 temperature sensor stabilizes. A constant current source was used to deliver heat to the sample, and the temperature rise is recorded over a period. Each measurement was repeated twice, and the average reading was used for results analysis.

2.4. SUSPENSION STABILITY TEST

The suspension stability test of the nanofluids was done by physically monitoring the settling of the nanoparticles in the nanofluid over time. A camera was used to capture a picture of the physical state of the nanofluid, which was used for the analysis of the nanofluid suspension stability.

3. RESULTS AND DISCUSSION

3.1. SHEAR STRESS VS SHEAR RATE

A sample of the shear stress vs shear rate plots for HOSO, Al2O3/HOSO-, TiO2/HOSO-, and MoS2/HOSO nanofluids for 0.5 wt.% and 4.0 wt.% concentrations are shown in Figures. 2 and 3, respectively. The shear stresses were measured for shear rates ranging from 0 to 100 1/s. The shear stress vs shear rate plot of HOSO base fluid and all three investigated HOSO nanofluids (Al2O3/HOSO-, TiO2/HOSO-, and MoS2/HOSO nanofluids) for all nanoparticles, weight concentrations, and temperature showed a similar linear trend typical for a Newtonian fluid. As shown in Figure 2 for 0.5 wt.%, shear stress increases linearly with an increase in shear rate and decreases with an increase in temperature for all three nanofluids. It is also observed that the shear stress of the nanofluids is more affected by temperature than by the type of nanoparticle. At a shear rate of 100 1/s, nanofluids with 0.5 wt. % nanoparticle concentration generated shear stresses of 5.76, 5.62, and 5.70 Pa for TiO2/HOSO, Al2O3/HOSO, and MoS2/HOSO nanofluids, respectively, at room temperature and 1.49, 1.44, and 1.47 Pa at 70 °C. All nanofluids showed similar shear stress, and the percentage increases were

approximately equal compared to the base fluid, while the change in shear stress was observed to drop significantly due to an increase in temperature. At higher wt. % concentration as shown in Figure 3, the proportionality of shear stress and shear rate is affected by the type of nanoparticle and test temperature. It is observed that HOSO-based nanofluid using TiO2 nanoparticles has the highest shear stress and percentage increase from that of the base fluid. At 100 1/s shear rate, shear stresses of 6.53, 5.9, and 5.96 Pa were obtained for TiO2/HOSO, Al2O3/HOSO, and MoS2/HOSO nanofluids, respectively, at room temperature and 1.66, 1.47, and 1.53 Pa at 70 °C. This is likely due to the mechanism behind functionality (association and entanglement and thickening mechanism) [22] on the type of nanoparticle and temperature as the wt. % concentration increases. Shear stress of HOSO nanofluids using TiO2, MoS2, and Al2O3 nanoparticles as additives increases comparatively to HOSO base fluid as nanoparticle wt. % concentration increases for a given shear rate and temperature. It can also be seen that TiO2/HOSO nanofluid gave the highest shear stress followed closely by both MoS2/HOSO and Al2O3/HOSO nanofluids. The shear stability of HOSO is not affected by the addition of nanoparticles for the range of wt. % concentrations and temperatures studied. The R square values were all above 0.99, showing a strong linear relationship between the shear stress and shear rate.

3.2. VISCOSITY AND VISCOSITY ENHANCEMENT OF BASE FLUID

The plots of viscosity versus temperature of HOSO base fluid and HOSO nanofluids are shown in Figures. 4, 5, and 6 for Al2O3/HOSO, TiO2/HOSO, and MoS2/HOSO nanofluids, respectively. The shear stress vs shear rate plots show a

pattern like that of Newtonian fluids; therefore, viscosities were determined from the plots. Viscosities of HOSO base fluid and HOSO nanofluids were calculated using Eq. (1) for all shear stress vs shear rate line plots, for all three nanofluids at all nanoparticle wt.% concentration and temperature. The figures show that viscosity for HOSO base fluid and all three nanofluids decreases exponentially with the increase in temperature.

Nanofluids with higher nanoparticle concentrations show a significant increase in viscosity compared to those with lower nanoparticle concentration and HOSO base fluid. The viscosity of Al2O3/HOSO, TiO2/HOSO, and MoS2/HOSO nanofluids and HOSO base fluid at room temperature shows a significant difference compared to those at 70 °C. This is likely due to the weakening of the solid-liquid interaction and reduction of the liquid shear stress leading to lower thickening and entanglement mechanisms. Also, a significant difference is observed in the plots due to the wt. % concentration increase at room temperature and the differences decrease as the temperature rises to 70 °C for TiO2/HOSO, compared to Al2O3/HOSO and MoS2/HOSO. Viscosity enhancement of HOSO base fluid using TiO2, MoS2, and Al2O3 nanoparticles as additives to the base fluid to form nanofluids is shown in Figure 7 for 1.0 and 3.5 wt. % in nanoparticle concentrations.

The viscosity enhancement of HOSO base fluid was calculated using Eq. (2) for nanoparticles and wt. % concentration at a temperature range from 25 to 70 °C. An increase in wt. % concentration of nanoparticles leads to an increase in viscosity enhancement. Maximum viscosity enhancement of HOSO base fluid was obtained by using TiO2 nanoparticles as additives which gave 11.5% and 8% enhancement at 3.5 and 1.0 wt. % concentration, respectively, at 50 °C, followed by using MoS2 which gave

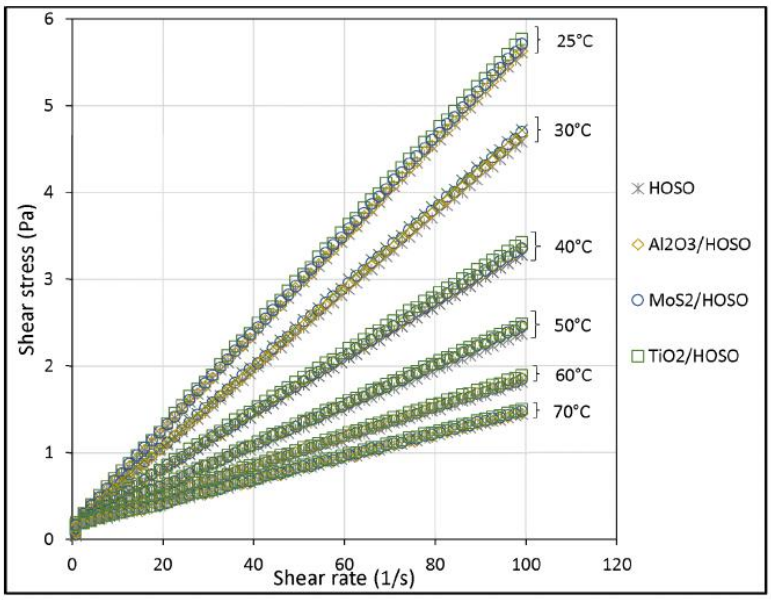

Figure 2. Shear stress vs shear rate of HOSO and Al2O3/HOSO, TiO2/HOSO, and MoS2/HOSO nanofluids at 0.5 wt.% conc. and temperature from 25 to 70 °C.

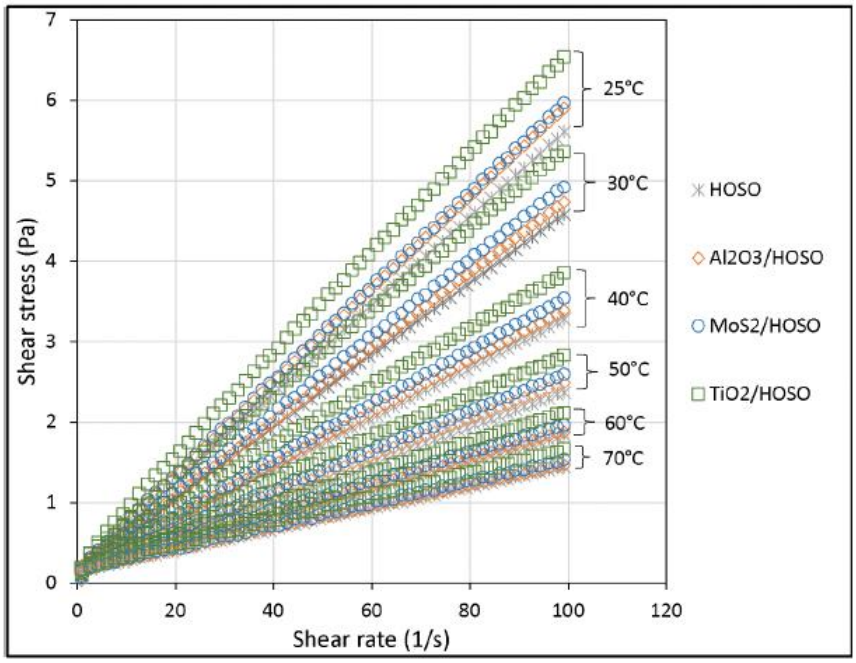

Figure 3. Shear stress vs shear rate of HOSO base fluid and Al2O3/HOSO,TiO2/HOSO, and MoS2/HOSO nanofluids at 4.0 wt.% conc.and temperature from 25 to 70 °C.

9.14% and 4.44% enhancement at 3.5 and 1.0 wt. % concentration, respectively, at 40 °C and 50 °C, and least enhancement occurred when Al2O3 nanoparticle was used as additives in the base fluid which gave 7.5% and 3.1% at 3.5 and 1.0 wt. % concentration, respectively, at 50 °C. Figure 7 shows an increase in viscosity enhancement for a given wt. % concentration with an increase in temperature up to 50 °C and decreases with further increase in temperature. This can be explained by a combination of association and entanglement mechanism, thickening mechanism, solid-liquid interaction, and reduction of the liquid shear stress.

$$\sigma = \mu\dot{\gamma} \tag{1}$$

$$\text{Enhancement (\%)} \quad {}^{\Delta\mu}/_{\mu} = \frac{\mu_{nanofluid} - \mu_{base\ fluid}}{\mu_{base\ fluid}} \times 100 \tag{2}$$

(σ is the shear stress (Pa), γ is the shear rate (1/s), and μ is the dynamic viscosity (Pa. s).)

3.3. THERMAL CONDUCTIVITY AND THERMAL CONDUCTIVITY ENHANCEMENT OF BASE FLUID

The plots of thermal conductivity vs temperature e are shown in Figs. 8, 9, and 10 for Al2O3/HOSO-, TiO2/HOSO-, and MoS2/HOSO nanofluid, respectively. Equation (3) shows how thermal conductivity is obtained for both the based fluid and nanofluids. From the figures, the thermal conductivity of HOSO base fluid decreases with a rise in temperature while that of nanofluids increases with a rise in temperature and an increase in nanoparticle weight concentration.

The structure of fatty acid in HOSO and Brownian motion of free moving particles can be used to explain the above trend observed. HOSO acts as a heat sink, and temperature rise tends to break the fatty acid structure rather than moving the molecules,

while in HOSO nanofluid, the movement and collision of free moving nanoparticles lead to energy transfer. The structure of fatty acid in HOSO and Brownian motion of free moving particles can be used to explain the above trend observed. HOSO acts as a heat sink, and temperature rise tends to break the fatty acid structure rather than moving the

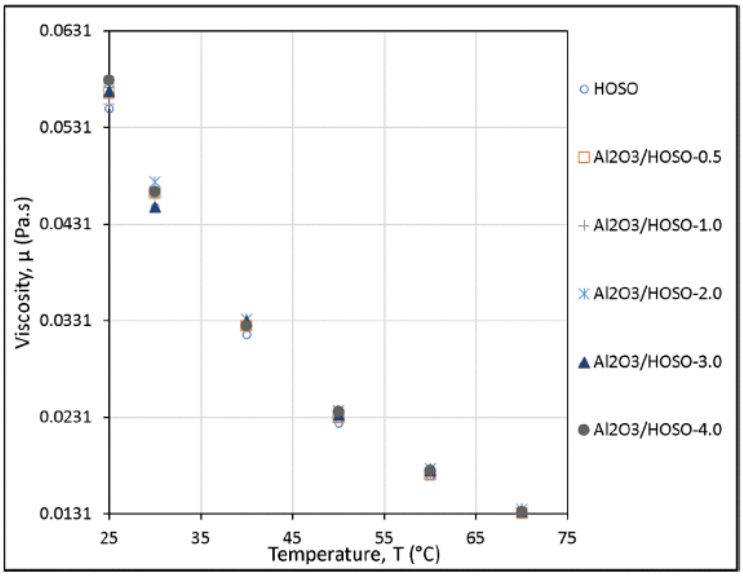

Figure 4. Viscosity vs temperature for HOSO and Al2O3/HOSO nanofluid from 0.5 to 4.0 wt.% concentration.

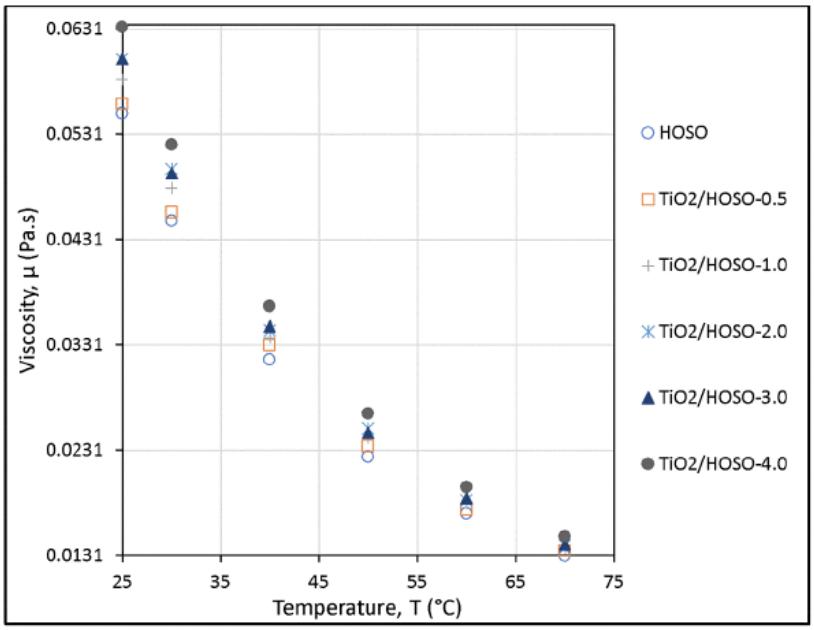

Figure 5. Viscosity vs temperature for HOSO and TiO2/HOSO nanofluid from 0.5 to 4.0 wt.% concentration.

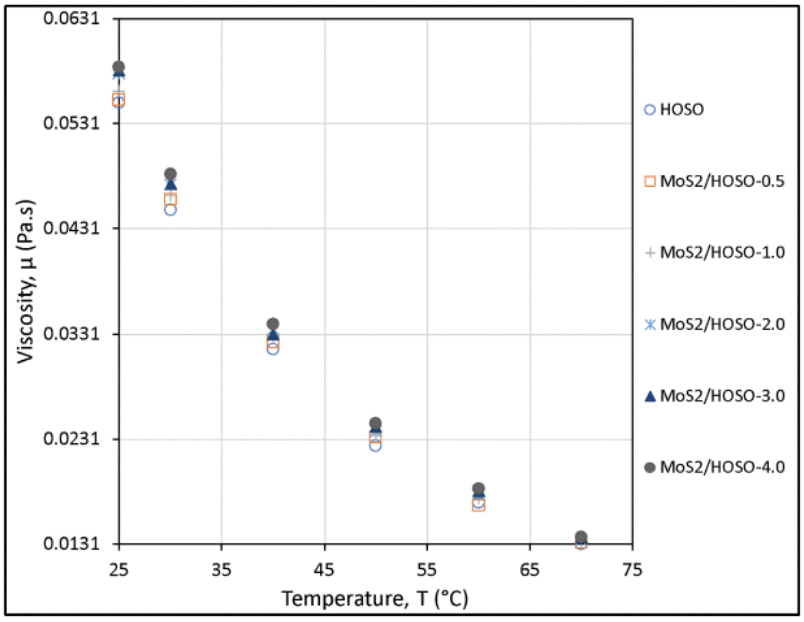

Figure 6. Viscosity vs temperature for HOSO and MoS2/HOSO nanofluid from 0.5 to 4.0 wt.% concentration.

molecules, while in HOSO nanofluid, the movement and collision of free moving nanoparticles lead to energy transfer. Also, temperature rise decreases the viscosity of HOSO making it easier for nanoparticles to move within the layers of HOSO in the nanofluid. The increase in the wt.% concentration increases clustering and bombardment of nanoparticles increasing heat transfer. It was observed that maximum thermal conductivity occurs at the maximum test temperature and nanoparticle wt. % concentration.

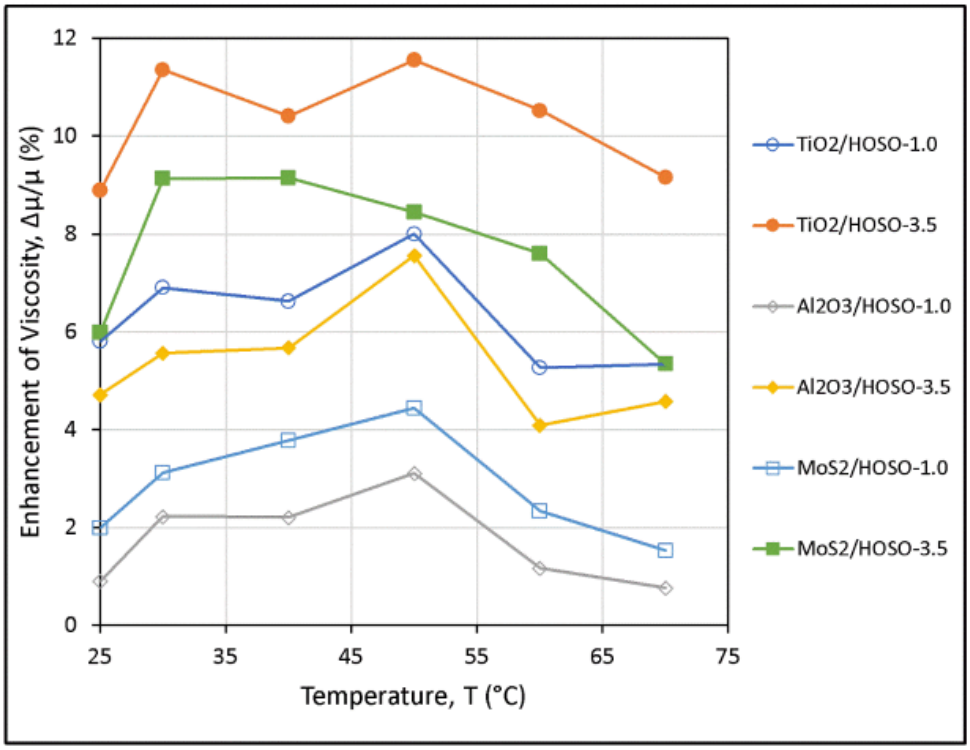

Figure 7. Viscosity enhancement vs temperature of HOSO base fluid using 1and 3.5 wt. % nanoparticle concentration.

Thermal conductivity was observed to be 0.275 w/mK for Al2O3/HOSO-, 0.271 w/mK for TiO2/HOSO-, and 0.276 w/mK for MoS2/HOSO nanofluids at 70 °C and 4.0

wt. % concentration. Thermal conductivity enhancement of HOSO nanofluid compared to the base fluid with an increase in temperature and nanoparticle wt.% concentration was obtained from Eq. (4) is shown in Figure 11. The plot shows that increasing nanoparticle wt.% concentration increases the Brownian motion and collision of the particles further enhances the thermal conductivity of the nanofluids. Also, a rise in temperature decreases the viscosity of nanofluids and weakens the friction within the HOSO layers, thus causing an increase in the enhancement of nanofluid thermal conductivity. It was observed that the thermal conductivity of HOSO can be enhanced to approximately 55% at a temperature of 70 °C and by increasing the nanoparticle up to 4.0 wt. % concentration.

$$k = \frac{q}{4\pi a} \tag{3}$$

$$\text{Enhancement}(\%)\ \Delta k/_k = \frac{k_{nanofluid} - k_{base\ fluid}}{k_{base\ fluid}} \times 100 \tag{4}$$

3.4. SUSPENSION STABILITY

The nanoparticle suspension stability is shown in Figure 12, for Al2O3/HOSO-, MoS2/HOSO-, and TiO2/HOSO nanofluid using 0.5, 2.0, and 4.0 wt.% concentration, respectively. The nanoparticles were observed to be stable for all weight concentrations up to 1 h except for TiO2-HOSO at 4.0 wt.% concentration.

It was also observed that nanoparticle suspension stability decreases with an increase in wt.% concentration. This trend can be possible due to the larger mass in the nanofluid, causing nanoparticles to push through the base fluid layers and agglomerate easily. Al2O3/HOSO nanofluid was stable for up to 3 days and started agglomeration for

larger weight concentration. MoS2/HOSO nanofluid maintained its stability and started agglomerating after 1 week and completely settled at 2 weeks. MoS2 showed longer stability in HOSO compared to Al2O3, and TiO2 showed the lowest stability in HOSO.

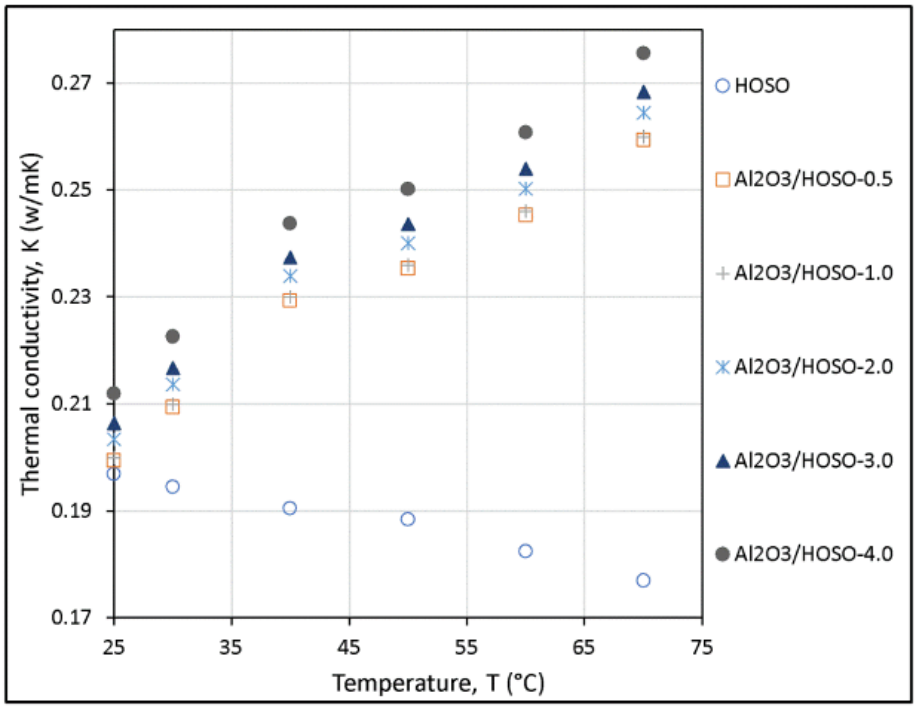

Figure 8. Thermal conductivity vs temperature for HOSO and Al2O3/HOSO nanofluid from 0.5 to 4.0 wt.% concentration.

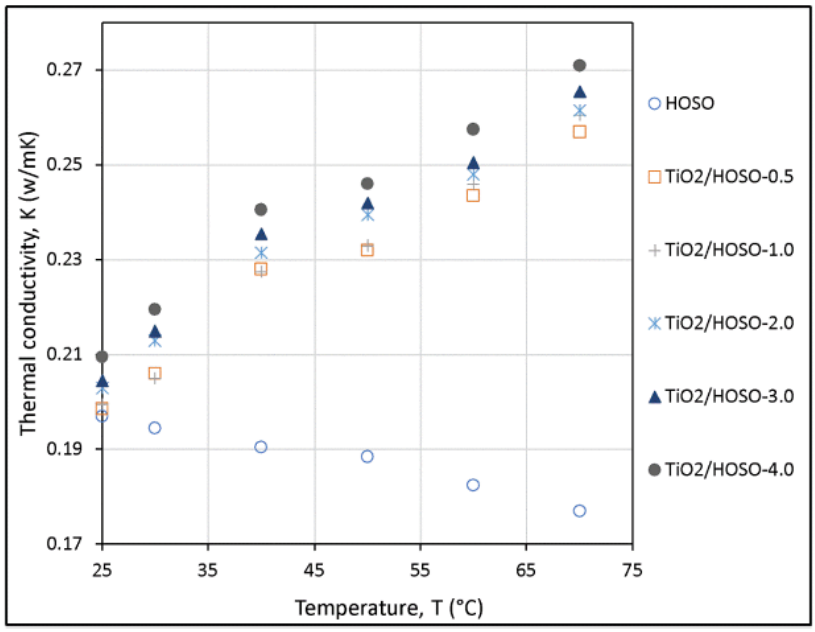

Figure 9. Thermal conductivity vs temperature for HOSO and TiO2/HOSO nanofluid from 0.5 to 4.0 wt.% concentration.

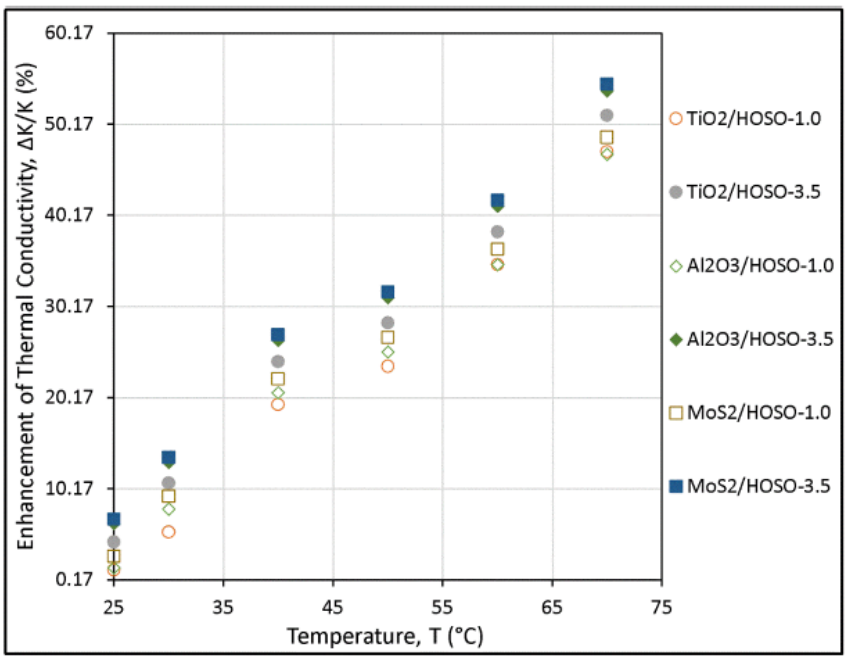

Figure 10. Thermal conductivity vs temperature for HOSO andMoS2/HOSOnanofluid from 0.5 to 4.0 wt.% concentration.

4. CONCLUSIONS

This study investigated shear stress vs shear rate, viscosity, thermal conductivity, and suspension stability of three vegetable oil-based nanofluids using high oleic soybean oil (HOSO) as the base fluid and Al2O3, MoS2, and TiO2 nanoparticles of the same 30 nm average nanoparticle size at varying weight concentration (0.5–4% wt.) and a temperature range from 25 to 70 °C, for use as cutting fluids in nanofluid minimum quantity lubrication (nMQL) machining of difficult-to-cut metals. The resulting nanofluids are designated as TiO2/HOSO, MoS2/HOSO, and Al2O3/HOSO nanofluids. From the results, the following conclusions are made. Shear stress vs shear rate plots of TiO2/HOSO, MoS2/HOSO, and Al2O3/HOSO nanofluids show an increasing linear trend typical of Newtonian fluids for all temperature range and percentage weight concentration investigated.

1. Shear stress of TiO2/HOSO, MoS2/HOSO, and Al2O3/HOSO nanofluids decreases exponentially with an increase in temperature.
2. TiO2/HOSO nanofluid generates the highest shear stress followed by MoS2/HOSO, Al2O3/HOSO, and HOSO base fluid in that order for all temperature and nanoparticle wt.% concentration; and shear stress increases with an increase in nanoparticle wt. concentration, the highest increase occurring at room temperature (25 °C).
3. The viscosity of TiO2/HOSO, MoS2/HOSO, and Al2O3/HOSO nanofluids and HOSO base fluid decreases exponentially with an increase in temperature, and

they increase with an increase in nanoparticle % wt. concentration from 0 to 4% wt.

4. The viscosity of HOSO base fluid can be enhanced using TiO2, MoS2, and Al2O3 nanoparticles as additives to form nanofluids.
5. Maximum viscosity enhancement of HOSO base fluid is obtained by using TiO2 nanoparticles as an additive to provide up to 11.5% and 8% enhancement at 3.5% wt. and 1% wt. concentration, respectively, at 50 °C; MoS2 nanoparticles can provide up to
6. 14% and 4.44% enhancement at 3.5% wt. and 1% weight concentration at 50 °C, respectively, while Al2O3 nanoparticles provide the least enhancement of 7.5% and 3.1% at 3.5% wt. and 1% wt. concentration, respectively, at 50 °C.
7. Thermal conductivity of TiO2/HOSO-, MoS2/HOSO-, and Al2O3/HOSO nanofluids increase with an increase in temperature and nanoparticle wt. concentration, while thermal conductivity of HOSO base fluid decreases with an increase in temperature. This is a very significant positive observation especially for machining difficult-to-cut metals that generate high heat that needs to be conducted away from the cutting zone.
8. Maximum thermal conductivity occurs at 70 °C and 4% wt. concentration for all three nanofluids investigated.
9. Maximum thermal conductivity enhancement of HOSO base fluid is obtained by using MoS2 nanoparticles as an additive which provides up to 55% enhancement at 70 °C and 4% wt., followed by Al2O3/HOSO and then TiO2/HOSO nanofluids.

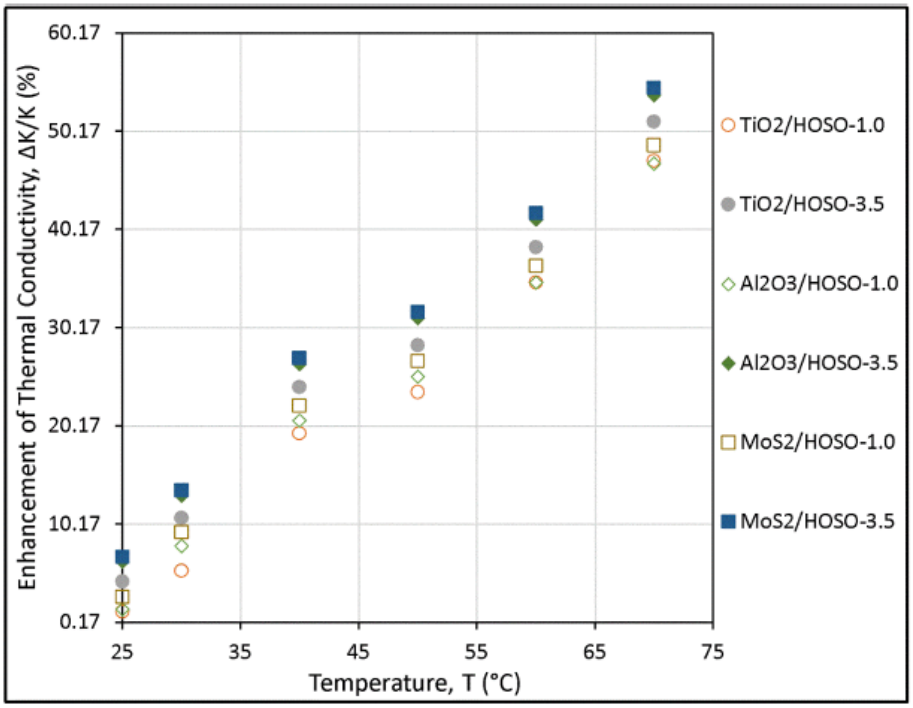

Figure 11. Enhancement of thermal conductivity vs temperature of Al2O3/HOSO, TiO2/HOSO, and MoS2/HOSO nanofluid for 1.0 to 3.5 wt.% concentration.

10. Maximum thermal conductivities obtained were 0.276, 0.275, and 0.271 for MoS2/HOSO-, Al2O3/HOSO-, and TiO2/HOSO nanofluids, respectively, at 70 °C and 4% wt. concentration.
11. Since of significant interest is an enhancement of thermal conductivity of HOSO vegetable oil, MoS2/HOSO nanofluid is recommended followed by Al2O3/HOSO nanofluid and then TiO2/HOSO nanofluid.
12. MoS2 nanoparticle remains stable in high oleic soybean oil for about 2 weeks, and it is more stable compared to Al2O3 nanoparticle and TiO2 nanoparticle which exhibit the lowest suspension stability in HOSO. The increase in nanoparticle weight concentration leads to poor suspension stability of the nanofluid.

13. To further enhance the viscosity and thermal conductivity of high oleic soybean oil, the authors propose to investigate MoS2, Al2O3, TiO2, and graphene nanofluids by extending nanoparticle weight concentration up to 8%.

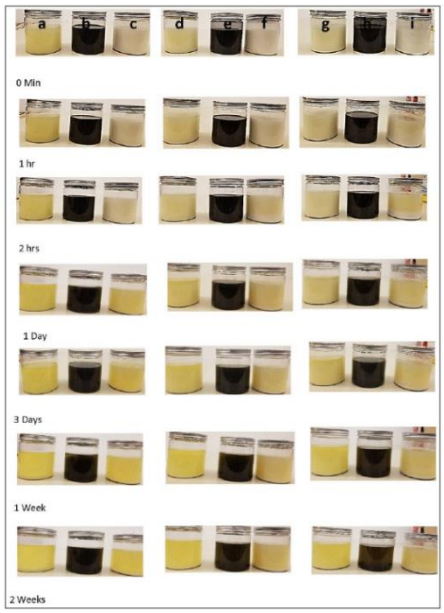

Figure 12. Suspension stability of nanoparticles in nanofluid at 0.5, 2.0, and 4.0 wt.% conc. (a Al2O3/HOSO-0.5%, b MoS2/HOSO-0.5%, c TiO2/HOSO-0.5%, d Al2O3/HOSO-2.0%, e MoS2/HOSO-2.0%, f TiO2/HOSO-2.0%, g Al2O3/HOSO-4.0%, h MoS2/HOSO-4.0%, i TiO2/HOSO-4.0%).

REFERENCES

1. Ahmadi MH, Mirlohi A, Alhuyi Nazari M, Ghasempour R (2018) A review of thermal conductivity of various nanofluids. J Mol Liq 265:181–188

2. Chetan BBC, Ghosh S, Rao PV (2016) Application of nanofluids during minimum quantity lubrication: a case study in turning process. Tribol Int 101:234–246. https://doi.org/10.1016/j.triboint.2016.04.019

3. Shokrani A, Dhokia V, Newman ST (2016) Investigation of the effects of cryogenic machining on surface integrity in CNC end milling of Ti-6Al-4V titanium alloy. J Manuf Process 21:172–179. https://doi.org/10.1016/j.jmapro.2015.12.002
4. Okafor AC, Jasra PM (2019) Effects of milling methods and cooling strategies on tool wear, chip morphology and surface roughness in high-speed end-milling of Inconel 718. Int J Mach Mach Mater 21:3. https://doi.org/10.1504/ijmmm.2019.098065

5. Corcione M (2011) Empirical correlating equations for predicting the effective thermal conductivity and dynamic viscosity of nanofluids. Energy Convers Manag 52–1:789–793. https://doi.org/10.1016/j.enconman.2010.06.072

6. Park KH, Suhaimi MA, Yang GD, Lee DY, Lee SW, Kwon P (2017) Milling of titanium alloy with cryogenic cooling and minimum quantity lubrication (MQL). Int J Precis EngManuf 18:5–14. https://doi.org/10.1007/s12541-017-0001-z

7. Sidik NAC, Samion S, Ghaderian J, Yazid MNAWM (2017) Recent progress on the application of nanofluids in minimum quantity lubrication machining: a review. Int J Heat Mass Transf 108:79–89

8. Behera BC, Chetan, Setti D, et al (2017) Spreadability studies of metalworking fluids on tool surface and its impact on minimum amount cooling and lubrication turning. J Mater Process Technol 244:1–16. https://doi.org/10.1016/j.jmatprotec.2017.01.016

9. Yuan S, Hou X, Wang L, Chen B (2018) Experimental investigation on the compatibility of nanoparticles with vegetable oils for nanofluid minimum quantity lubrication machining. Tribol Lett 66. https://doi.org/10.1007/s11249-018-1059-1

10. Li G, Yi S, Li N, Pan W, Wen C, Ding S (2019) Quantitative analysis of cooling and lubricating effects of graphene oxide nanofluids in machining titanium alloy Ti6Al4V. J Mater Process Technol 271:584–598. https://doi.org/10.1016/j.jmatprotec.2019.04.035

11. Okafor AC, Nwoguh TO (2020) A study of viscosity and thermal conductivity of vegetable oils as base cutting fluids for minimum quantity lubrication machining of difficult-to-cut metals. Int J Adv Manuf Technol 106:1121–1131. https://doi.org/10.1007/s00170-019-04611-3

12. Okafor AC, Nwoguh TO (2020) Comparative evaluation of soybean oil based MQL flow rates and emulsion flood cooling strategy in high-speed face milling of Inconel 718. Int J Adv Manuf Technol 107:3779–3793. https://doi.org/10.1007/s00170-020-05248-3

13. Ezugwu EO, Bonney J (2004) Effect of high-pressure coolant supply when machining nickel-base, Inconel 718, alloy with coated carbide tools. J Mater Process Technol 153–154:1045–1050. https://doi.org/10.1016/j.jmatprotec.2004.04.329

14. Martini A, Ramasamy US, LenM(2018) Review of viscosity modifier lubricant additives. Tribol Lett 66:58, 1–14. https://doi.org/10.1007/s11249-018-1007-0

15. Mishra PC, Mukherjee S, Nayak SK, Panda A (2014) A brief review on the viscosity of

16. Pryazhnikov MI, Minakov AV, Rudyak VY, Guzei DV (2017) Thermal conductivity

17. Asadi M, Asadi A, Aberoumand S (2018) An experimental and theoretical investigation on the effects of adding hybrid nanoparticles on heat transfer efficiency and pumping power of an oil-based nanofluid as a coolant fluid. Int J Refrig 89:83–92. https://doi.org/10.1016/j.ijrefrig.2018.03.014

18. Omrani AN, Esmaeilzadeh E, Jafari M, Behzadmehr A (2019) Effects of multi-walled carbon nanotubes shape and size on thermal conductivity and viscosity of nanofluids. Diam Relat Mater 93:96–104. https://doi.org/10.1016/j.diamond.2019.02.002

19. Chandrasekar M, Suresh S, Chandra Bose A (2010) Experimental investigations and theoretical determination of thermal conductivity and viscosity of Al2O3/waternanofluid. Exp Thermal Fluid Sci 34:210–216. https://doi.org/10.1016/j.expthermflusci.2009.10.022

20. Vajjha RS, Das DK (2009) Experimental determination of thermal conductivity of three nanofluids and development of new correlations. Int J Heat Mass Transf 52:4675–4682. https://doi.org/10.1016/j.ijheatmasstransfer.2009.06.027

21. Bashirnezhad K, Bazri S, Safaei MR, Goodarzi M, Dahari M, Mahian O, Dalkılıça AS, Wongwises S (2016) Viscosity of nanofluids: a review of recent experimental studies. Int Commun Heat Mass Transf 73:114–123. https://doi.org/10.1016/j.icheatmasstransfer.2016.02.005

SECTION

5. CONCLUSION AND RECOMMENDATION

5.1. CONCLUSION

In this research, corrosion analysis of hot stamped Usibor^{R} 1500 coated with two different coating weights AS150 (36µm) and AS80 (20µm) using the Interdiffusion Layer process is studied. The result shows: Both coating weights AS150 and AS80 exhibited similar excellent perforation corrosion resistance compared to 22MnB5 (Bare Usibor) due to highly protective corrosion products of Aluminum-Silicon (AlSi). Both AS80 and AS150 show maximum depth of corrosion attack of less than 200 µm compared to 22MnB5 that has maximum depth of corrosion attack of approximately 900 µm. The Aluminum-Silicon coating of Usibor^{R} 1500 serves as a barrier to oxygen reduction to a greater magnitude even when the corrosion element is perceived to be gradually initiating corrosion attack into steel cavities of the alloy.

The result of the cosmetic corrosion test shows Usibor AS150 displayed better resistance to cosmetic corrosion than Usibor AS80, in terms of mean and maximum scribed creep back (mm) of scribed lines, due to the presence of aluminum -rich protective corrosion product. Thicker coating layer thus implies the thicker the coating weight the better the corrosion resistance. The result agrees with Mizuno [25] finding that an increase in the coating thickness improves corrosion resistance.

Successful spot welding operations can be carried out to marry a stack up of 1.5 mm gauges of USIBOR 1500 with coating weights of AS80 and AS150 as both coating

weights exhibited good spot-weld nugget diameter and metallurgy, the weld nugget diameter were all trending above 4.9 mm minimum weld nugget diameter which is most suitable for automotive industry application, and a good indication that AS150 and AS80 can be spot-welded to produce a desirable weld strength for either AS80 or AS150 stack up as may be applicable in automotive industries.

Tensile Shear Strength (TSS) for AS150 and AS80 increases nonlinearly with increase in weld diameter from approximately 15,000 N (at weld nugget dia. of 4.5 mm) to approximately 27,500 N (at weld nugget dia. of 7.5mm), similar characteristic was observed with Cross-Tensile Strength (CTS). Both AS150 and AS80 exhibited good spot-welding strength and metallurgy, the weld strengths were all trending above 4.9mm minimum weld diameter threshold which is a good indication that AS150 and AS80 can be spot welded at desirable weld strengths applicable in automotive industries under minimum weld current range of 2.1kA for AS80 and 1.8kA for AS150.

2000 good spot welds were obtained on each coupon with AS80 and AS150 coating weights, before the spot welding was terminated, as all weld nugget diameters were above 4.9 mm defined as the minimum weld diameter for the investigated resistance spot welding and is acceptable for automotive industry applications.

Nugget diameter (electrode life) at welding current of 7.5 KA decreases gradually with increasing spot weld count, from nugget diameter of about 7 mm initially, which is above the 4.9 mm minimum weld nugget diameter, to a nugget diameter about 6.5 mm at 2000 spot weld count for both AS150 and AS80 coating weights.

Finally, shear stress of TiO2/HOSO, MoS2/HOSO, and Al2O3/HOSO nanofluids decreases exponentially with an increase in temperature. TiO2/HOSO nanofluid

generates the highest shear stress followed by MoS2/HOSO, Al2O3/HOSO, and HOSO base fluid in that order for all temperature and nanoparticle wt.% concentration; and shear stress increases with an increase in nanoparticle wt. concentration, the highest increase occurring at room temperature (25 °C). The viscosity of TiO2/HOSO, MoS2/HOSO, and Al2O3/HOSO nanofluids and HOSO base fluid decreases exponentially with an increase in temperature, and they increase with an increase in nanoparticle % wt. concentration from 0 to 4% wt. The viscosity of HOSO base fluid can be enhanced using TiO2, MoS2, and Al2O3 nanoparticles as additives to form nanofluids. Maximum viscosity enhancement of HOSO base fluid is obtained by using TiO2 nanoparticles as an additive to provide up to 11.5% and 8% enhancement at 3.5% wt. and 1% wt. concentration, respectively, at 50 °C; MoS2 nanoparticles can provide up to 14% and 4.44% enhancement at 3.5% wt. and 1% weight concentration at 50 °C, respectively, while Al2O3 nanoparticles provide the least enhancement of 7.5% and 3.1% at 3.5% wt. and 1% wt. concentration, respectively, at 50 °C. Thermal conductivity of TiO2/HOSO-, MoS2/HOSO-, and Al2O3/HOSO nanofluids increase with an increase in temperature and nanoparticle wt. concentration, while thermal conductivity of HOSO base fluid decreases with an increase in temperature. This is a very significant positive observation especially for machining difficult-to-cut metals that generate high heat that needs to be conducted away from the cutting zone.

5.2. RECOMMENDATION

Coupled with cost reduction opportunities, further research work should be carried out to study the feasibility of spot welding a stack up of AS80 and AS80 with

1.5mm and 1mm gage to avoid unexpected production or parts performance issues. Also, corrosion studies of resistance spot welded joints of USIBOR 150 with AS80 and AS150 coatings to ascertain their corrosion resistance, types, and mechanism

VITA

Hilary Anayochukwu Onyishi was born in Enugu, Nigeria. He earned his bachelor's degree in mechanical engineering at the Nnamdi Azikiwe University Awka, Nigeria in 2006. He worked as Project Engineer with ExxonMobil Nigeria up to 2009. He enrolled as a master's student in the Mechanical and Aerospace Engineering department at Missouri University of Science and Technology Rolla beginning January 2010. During his masters, he served as a Graduate Research Assistant and Graduate Teaching Assistant with the Department of Mechanical and Aerospace Engineering at Missouri University of Science and Technology Rolla. In May 2012, he joined Ford Motors Company in Dearborn Michigan as Design and Release Engineer and at the same time, was admitted in PhD program with Department of Mechanical Engineering in 2015. In 2019, he joined Collins Aerospace as a Project Engineering Manager in Windsor Locks, Connecticut. In May 2024 he received his PhD in Mechanical Engineering from Missouri University of Science and Technology.